6-20-2019 2:00 PM

Characterization of the Growth Hormone Secretagogue Receptor in Dilated Cardiomyopathy

Maedeh Naghibosadat, *The University of Western Ontario*

Supervisor: Dr. Savita Dhanvantari, *Imaging Program, Lawson Health Research Institute, London ON*
: Dr. Lisa Hoffman, *Imaging Program, Lawson Health Research Institute, London ON*
A thesis submitted in partial fulfillment of the requirements for the Master of Science degree in Pathology and Laboratory Medicine

Abstract

Duchenne muscular dystrophy (DMD) is a severe neuromuscular disease of skeletal and myocardial degeneration. Eventually, dilated cardiomyopathy develops from ischemia, inflammation and fibrosis. Due to the high mortality rate, there is an emerging need to diagnose DMD cardiomyopathy at early stages. Currently, DMD cardiomyopathy is diagnosed by imaging investigations and detection of circulating biomarkers. However, current imaging strategies detect functional and morphological changes but fall short in detecting molecular changes that underlie this disease. Circulating biomarkers provide information on the molecular level, but they are not cardiac-specific. Therefore, there is an emerging need for a biomarker that is endogenous to cardiac tissues. The growth hormone secretagogue receptor (GHSR) and its ligand, ghrelin are produced by both cardiomyocytes and vascular endothelial cells and could be an indicator of DMD cardiomyopathy. The work described in this thesis sought to characterize GHSR as a cardiac-localized biomarker in DMD cardiomyopathy. Histopathology and confocal imaging using a novel fluorescent ghrelin analog, Cy5-ghrelin (1-19), were used to investigate changes in cardiac tissue architecture and GHSR and inflammatory markers in the *mdx:utrn*$^{-/-}$ mouse model of DMD. My studies show that GHSR is elevated in *mdx:utrn*$^{-/-}$ myocardial tissues and correlate strongly with the macrophage marker F4-80 and the pro-inflammatory cytokine IL-6. Interestingly, I also show that both ghrelin and des-acyl ghrelin bind to sites in large cardiac vessels of *mdx:utrn*$^{-/-}$ which might be an indicator of vascular inflammation. Finally, my project shows the first report of GHSR in cardiac macrophages. In summary, my work suggests that, in dilated cardiomyopathy, elevations in GHSR correlate with the inflammatory phenotype as mediated by both the myocardium and macrophages.

Keywords:

Dilated cardiomyopathy, Duchenne Muscular Dystrophy, GHSR, Inflammation, Biomarker, *mdx:utrn*$^{-/}$

Lay Summary

Heart disease is the leading cause of death in Canada. It is usually diagnosed by imaging, such as ultrasound. However, this kind of imaging can miss small changes in the heart that lead to heart disease. My work has addressed this issue by identifying a protein located in the heart muscle that may indicate the onset of heart disease. I showed that this protein, called GHSR, is increased in the heart in a mouse model of heart disease, along with the degree of inflammation in the heart. My research has shown that there may be more sensitive ways of detecting heart disease, so that it may be diagnosed at earlier stages.

Co-Authorship Statement

Mr. Andrew Bondoc (Department of Medical Biophysics) was responsible for mouse breeding, genotyping, echocardiography and heart dissection. The Robarts Pathology Facility performed paraffin embedding of mouse hearts, sectioning and Masson's Trichrome and H& E staining. Tyler Lalonde and Carlie Charron (Department of Chemistry) synthesized the Cy5-ghrelin (1-19) and Cy3-des-acyl ghrelin (1-19) probes.

Acknowledgments

First and foremost, I would like to express my sincere appreciation to my supervisors, Dr. Savita Dhanvantari and Dr. Lisa Hoffman for giving me the opportunity to work in the multidisciplinary lab and, also, for their valuable support and mentorship during my master's program. Savita has also always kept an open door and aided me in all of my setbacks with a positive mind and a healthy attitude towards finding solutions. I am truly grateful for all she did during my graduate experience and this thesis is dedicated to her.

I would also like to thank my advisory committee members Dr. Dale Laird, Dr. Zia Khan, and Dr. Geoff Pickering for providing constructive feedback and assistance through my research.

I would like to thank Dr. Patti Kiser for providing helpful suggestions and input on histology interpretation, and Dr. Tianqing Peng for the kind gift of mouse cardiac microvascular endothelial cells.

Additionally, a lot of gratitude goes to Farzad Asadi, who helped me with all the steps involved in imaging and image analysis. Thank you for helping me with generously sharing your valuable knowledge.

Also, my thanks go to all the past and present members in Dhanvantari and Hoffman Labs. Special thanks to Rebecca Sullivan who not only helped with my research but also with making a lot of good moments and memories that I will never forget.

I also would like to acknowledge Robarts Pathology facility especially the help and support from Caroline O'Neil and Dr. John- Michael Arpino.

Last but certainly not least, I would like to send a huge thank-you to my family for their endless support. I am grateful for all you did for me.

I would like to acknowledge funding support from Collaborative Specialization in Musculoskeletal Health Research Training Program and Western Graduate Research Scholarship. I also would like to thank the Collaborative Program in Molecular Imaging and Pathology and Laboratory Medicine department at Western University.

Table of Contents

List of Tables

List of Figures

List of Abbreviations

2D	Two-Dimensional
3D	Three-Dimensional
AKT	Protein Kinase B
ANOVA	Analysis of Variance
ARVC	Arrhythmogenic right ventricular cardiomyopathy
ATP	Adenosine Triphosphate
BMD	Becker muscular dystrophy
BNP	B-Type Natriuretic Peptide
BCA	Bicinchoninic acid
BSA	Bovine Serum Albumin
Ca^{2+}	Calcium Ion
$CaCl_2$	Calcium Chloride
CD4	Cluster of Differentiation 4
CD8	Cluster of Differentiation 8
CD31	Cluster of Differentiation 31
CD36	Cluster of Differentiation 36 (AKA Fatty Acid Translocase)
CT	Computed Tomography
CVD	Cardiovascular disease
Cy3	Cyanine3
Cy5	Cyanine5
DAPI	4’,6-diamidino-2-phenylindole

DAPC	Dystrophin-associated protein
DCM	Dilated cardiomyopathy
DMD	Duchenne Muscular Dystrophy
DMEM	Dulbecco's Modified Eagle Medium
ECG	Electrocardiography
ECM	Extracellular matrix
EDTA	Ethylenediaminetetraacetic Acid
EF	Ejection Fraction
ELISA	Enzyme-Linked Immunosorbent Assay
ER	Endoplasmic Reticulum
ERK1	Extracellular signal-regulated kinase 1
ERK2	Extracellular signal-regulated kinase 2
FA	Fatty Acid
FBS	Fetal Bovine Serum
FDG	Fluorodeoxyglucose
FITC	Fluorescein Isothiocyanate
FOV	Field of View
GH	Growth Hormone
GHSR	Growth Hormone Secretagogue Receptor
GOAT	Ghrelin O-acyltransferase
GPCR	G-Protein Coupled Receptor
HCM	Hypertrophic cardiomyopathy
H&E	Hematoxylin and Eosin
HF	Heart Failure

HRP	Horseradish peroxidase
HUVEC	Human Umbilical Vein Endothelial Cell
ICAM-1	Intercellular Adhesion Molecule 1
IF	Immunofluorescence
IGF-1	Insulin-like growth factor 1
IgG	Immunoglobulin G
IL-1	Interleukin 1
IL-6	Interleukin 6
IL-8	Interleukin 8
IP3	Inositol triphosphate
LV	Left Ventricle
LVEF	Left ventricular Ejection Fraction
MAPK	Mitogen-Activated Protein Kinase
MCEC	Mouse cardiac microvascular endothelial cells
mdx	X Chromosome-Linked Muscular Dystrophy Mouse
mdx:utrn$^{+/-}$	Dystrophin-Knockout, Utrophin-Heterozygous Mouse
mdx:utrn$^{-/-}$	Dystrophin/Utrophin Double-Knockout Mouse
$MgCl_2$	Magnesium Chloride
Micro-CT	X-Ray Micro-Computed Tomography
MRI	Magnetic Resonance Imaging
mRNA	Messenger Ribonucleic Acid
NCBS	Newborn Calf Serum
NF-kB	Nuclear factor kappa-light-chain-enhancer of activated B cells
NO	Nitric Oxide

nNOS	Neuronal nitric oxide synthase
NT-pro-BNP	N-terminal pro-BNP
PBS	Phosphate Buffered Solution
PCC	Pearson's correlation coefficient
PCR	Polymerase chain reaction
PET	Positron Emission Tomography
PFA	Paraformaldehyde
PI3K	Phosphoinositide 3-Kinase
PIP2	Phosphatidylinositol 4,5-bisphosphate
PKC	Protein Kinase C
PLC	Phospholipase C
PVDF	Polyvinylidene difluoride
RCM	Restrictive cardiomyopathy
RIPA	Radioimmunoprecipitation assay
ROI	Region of Interest
RT-PCR	Reverse Transcriptase Polymerase Chain Reaction
SEM	Standard Error of the Mean
SER	Smooth endoplasmic reticulum
siRNA	Small Interfering Ribonucleic Acid
TNF-α	Tumor necrosis factor alpha
Th1	T-helper cells type-1
TBS	Tris-buffered saline
TBST	Tris-buffered saline-Tween
TLR	Toll-like receptor

TRITC	Tetramethylrhodamine Isothiocyanate
utrn	Utrophin
WT	Wild type

List of Appendices

Chapter 1

1 Introduction

1.1 Significance of the study

The heart is a muscular organ that pumps blood through the blood vessels of the body. In doing so, oxygen and nutrients are delivered, and metabolites are excreted. When the cells that make up the muscular portion of the heart, the cardiomyocytes, become dysfunctional, the heart becomes inefficient in its ability to pump blood, and the result is cardiomyopathy. There is a critical need to detect cardiomyopathy in its earlier stages, prior to the onset of overt symptoms. To address this need, our lab is developing new ways for the molecular imaging of the heart both *in situ* and *in vivo*. We have identified a possible biomarker of heart disease, the growth hormone secretagogue receptor (GHSR) and its ligand, ghrelin. Our lab has developed ghrelin analogs as molecular imaging tools that enable the imaging of GHSR *in vivo* through PET imaging and *in situ* through fluorescence microscopy of tissues. The work described in this thesis uses fluorescence molecular imaging to show that GHSR is elevated in a type of highly inflammatory and fibrotic dilated cardiomyopathy in a mouse model of muscular dystrophy, implicating the ghrelin/GHSR system as a biomarker in cardiomyopathy.

1.2 Cardiovascular disease

Cardiovascular disease (CVD) remains one of the greatest burdens of human disease and mortality globally[1]. In Canada, CVD is responsible for 19.7% of total annual death. Therefore, CVD places a heavy burden on the Canadian health care system which is estimated at $29 billion per year.[2] [3]

A wide array of conditions is classified as cardiovascular disease: peripheral blood vessel diseases, coronary artery diseases, arrhythmia, inflammatory heart disease and cardiomyopathy. To diagnose and treat each of these complex conditions, innovative approaches are required .[4] [5] Although coronary artery disease is the largest contributor to cardiovascular diseases, cardiomyopathies are clinically very devastating.[6] For example, 50% of cardiomyopathy patients die suddenly in their childhood or adolescence.[7]

1.3 Cardiomyopathies

Cardiomyopathies are structural myocardium abnormalities associated with cardiac dysfunction. Cardiomyopathies are categorized based on their morphology and function into hypertrophic, restrictive, dilative and arrhythmogenic right ventricular subtypes which might overlap genetically and phenotypically. [2] [8]

Hypertrophic cardiomyopathy is a disorder in which the ventricular wall thickness or mass is increased in the absence of a loading condition such as hypertension or valve disease. Myocyte hypertrophy occurs due to interstitial infiltration or intracellular accumulation of metabolic substrates.[9] [10] [11]

Restrictive cardiomyopathy refers to a pattern of ventricular filling that results in myocardium stiffness and causes a precipitous rise in ventricular pressure. RCM is difficult

to define since it occurs in numerous pathologies. But based on more specific classification, RCM is characterized by restrictive ventricular physiology in the presence of reduced systolic and diastolic volume with normal ventricular wall thickness. [12] [13] [14]

Arrhythmogenic right ventricular cardiomyopathy is defined by progressive substitution of right ventricular myocardium by adipose and fibrotic tissue with associated arrhythmia. These pathologic and histologic abnormalities are a result of disruptions to the inflow and outflow of blood through the right ventricle. [8] [15] [16] [17]

Dilated cardiomyopathy (DCM) is the most common subtype of cardiomyopathy due to its involvement with other diseases and it is the focus of this thesis.

1.4 Dilated Cardiomyopathies

DCM is a serious clinical concern due to its high prevalence and the high likelihood of heart failure (HF) in the later stages of the patient's life. The prevalence of DCM is estimated to be at least 1:2500; it is the third most common cause of heart failure and the most frequent cause of heart transplantation.[2] [18] However, DCM is underdiagnosed as some patients remain asymptomatic until marked ventricular dysfunction takes place; therefore, the prevalence may be as high as 1:250.[19] [20]

DCM is characterized by dilation of the left ventricle and systolic dysfunction. The ventricular myocardium, mainly the left ventricle, undergoes a combination of thinning and stretching which results in chamber enlargement and impaired contractility. This structural change leaves the patients at higher risk of HF which could spread to the other heart chambers. The DCM patients suffer from symptoms such as swelling of the lower

extremities, fatigue, shortness of breath, arrhythmia and valve problems.[21] The typical age of occurrence is between 20 to 60 years, and it is more prevalent in men than women. [22 23] DCM could be genetic and non-genetic. The non-genetic DCM may occur as a result of bacterial and viral infections or autoimmunity. [19 24] In genetic DCM, the mode of inheritance is typically autosomal and X-linked. The autosomal forms of DCM are caused by mutations in the genes that encode cytoskeletal (actin, myosin, tropomyosin, troponin I, troponin C, troponin T and vinculin), sarcomeric (sarcoglycan) and nuclear (lamin) and Z-band (titin) proteins. DCM also occurs in mitochondrial cytopathies.[17 19 24] Additionally, neuromuscular disorders such as Duchenne muscular dystrophy (DMD) and Becker muscular dystrophy (BMD) are X-linked muscular disorders which exhibit the DCM phenotype. [21 25] The focus of this thesis is DMD dilated cardiomyopathy.

1.5 DMD Dilated Cardiomyopathy

1.5.1 Duchenne Muscular Dystrophy

Duchenne muscular dystrophy (DMD) affects approximately 30,000 boys in North America, making it the most fatal disorder in early childhood.[26] It is an X-linked neuromuscular disease caused by mutations in the gene encoding dystrophin.

Dystrophin is one of the largest human proteins with a molecular weight of 427 kDa and is located within myocytes on the cytosolic side of the sarcolemma. Dystrophin acts as a bridge to connect the cytoskeletal F-actin to laminin in the extracellular matrix and is an important component of the dystrophin-associated protein complex or DAPC, that is also composed of dystroglycans, dystrobrevins, sarcoglycans, and syntrophins **(Figure 1)**. This

vital complex is a crucial link between the extracellular matrix (ECM) and the intracellular actin cytoskeleton and serves two functions: to maintain the structural integrity of the muscle fiber and to act as a scaffold for signaling proteins. Through interactions with dystrophin, several structural proteins provide stability, deformability and muscle integrity during skeletal muscle and cardiac contraction.[27] [28] A major signaling protein is neuronal nitric oxide synthase (nNOS), which is localized to the sarcolemma by dystrophin and catalyzes the synthesis of nitric oxide (NO), which facilitates vasorelaxation.

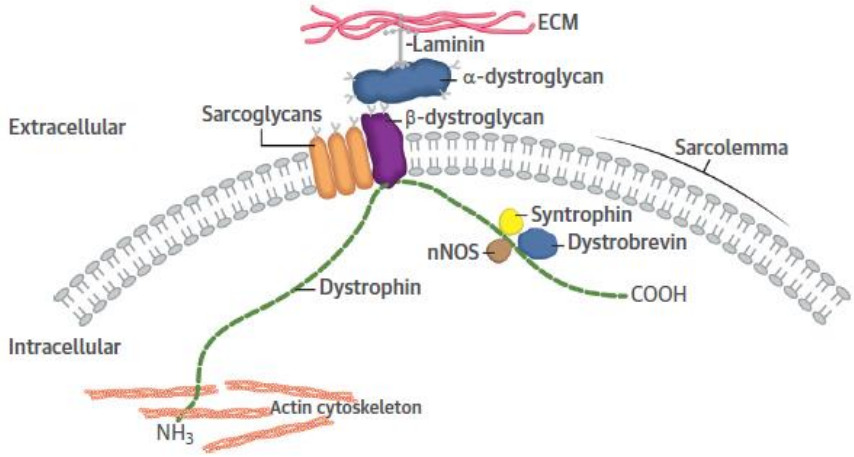

Figure 1: **Dystrophin links the ECM to cytoskeletal and signaling proteins**. This schematic illustrates the key location of dystrophin (green) at the sarcolemma of a myocyte, where it mediates interactions between the DAPC, the actin cytoskeleton and the intracellular signaling protein nNOS. [29] [30]

1.5.2 DMD Cardiac Pathology

The absence of dystrophin in skeletal muscle is the cause of Duchenne muscular dystrophy (DMD). One complication of DMD is dilated cardiomyopathy, characterized by a combination of ischemia, inflammation and fibrosis that is caused by an absence of

dystrophin in cardiomyocytes. These cardiac cells comprise the involuntary striated muscle (myocardium). Compared to skeletal myocytes, cardiomyocytes are short and branched and connected to their neighbors via intercalated disks, forming a strong, contractile muscle network.

Located within the sarcolemma of cardiomyocytes are L-type calcium channels which promote the influx of calcium ions from the extracellular matrix into the cells and contribute to the depolarization of the cardiomyocytes to maintain and generate contractile action.[31] The absence of dystrophin leads to the loss of integrity of the sarcolemma and shearing during myofiber contraction.[32 33] The damaged membrane allows for abnormal calcium ion influx that activates calpain proteases, which can auto-digest the cardiomyocytes. Calpain proteases also degrade cardiac troponin I, part of the troponin-actin-tropomyosin complex that mediates contractility.[27 34]

The abnormal calcium flow in cardiomyocytes also increases the level of reactive oxygen species, which stimulates the NF-κB signaling pathway, triggering the release of pro-inflammatory cytokines and resulting in immune response at the site. Subsequently, macrophages are recruited to the tissue for cell debris removal. Macrophages also attack the cardiac myofibers, thus exacerbating the sarcolemmal damage and leading to myonecrosis. Macrophages are the most abundant immune cells in DMD cardiac muscle and both M1 (pro-inflammatory) and M2 (regenerative) phenotypes are present at the site of cardiac injury. T-cells, B-cells and dendritic cells also found at the site, with $CD4^+$ T-cells being predominant to $CD8^+$ T-cells in DMD heart. Furthermore, in the process of myonecrosis, inflammatory macrophages release pro-inflammatory cytokines, which

triggers the fibroblasts in the extracellular matrix to produce collagen, leading to fibrosis.[35] [36] [37]

The pro-inflammatory cytokines TNF-α and IL-6 are elevated in the plasma of DMD patients.[38] TNF-α is associated with T-helper cells type-1 (Th1) and is upregulated 1000 times in DMD patients compared to healthy people. Studies have shown higher mRNA expression of TNF-α in the lymphocytes of DMD patients.[39] As well, in a mouse model of DMD, the diaphragm contains a significant amount of TNF-α mRNA, and TNF-α colocalizes strongly with macrophage infiltrates.[40]

IL-6 is another pro-inflammatory cytokine that is elevated in DMD patients. It is associated with T- helper cells type 2 (Th2). IL-6 exerts its pro-inflammatory effects via activation of the NF-κB pathway.[40] The concentration IL-6 is 4 times higher in the serum of DMD patients compared to the aged-matched controls. The levels of IL-6 mRNA in DMD skeletal muscles is significantly higher than in healthy muscles.[41] However, whether IL-6 or TNF-α is elevated in the DMD heart is not known.

Dystrophin also plays a role in maintaining adequate blood flow in the muscle through regulation of nNOS. Without dystrophin, nNOS does not attach properly to the sarcolemma; instead, it is mislocalized to the cytosol, where it activates metabolites that function in vasoconstriction, leading to inadequate blood flow and muscle ischemia. In addition, dystrophin deficiency in vascular smooth muscle cells also negatively impacts vasoregulation.[42] [43]

As a result of progressive loss of contractile function, increasing fibrosis and ischemia, the cardiac muscle regenerative capacity decreases with age, and the cardiac myofibers are

gradually replaced by connective and adipose tissues, [44] [45] eventually resulting in conduction defects and dilated cardiomyopathy after 10 years of age.[46] The progression of this cardiac defects worsen over time and will be present in all patients by 18 years of age and leading progressively to heart failure and is present in about 90% of patients. Initially, DMD patients have a normal heart but eventually, the inferobasal wall becomes fibrotic leading to hyper-trabeculation and dysfunction of the left ventricle which results in decreased contractility. Unfortunately, the cardiac complication of DMD is largely asymptomatic until heart function is severely hindered. [26] [27] [33] [47]

1.5.3 Pre-clinical models of DMD

Animal models play a vital role in pre-clinical diagnostic and therapeutic research and provide insights into disease mechanisms. To study DMD, there are numerous mammalian models, including canine, feline and mouse models. The canine X-linked muscular dystrophy model demonstrates a rapid progressive muscular phenotype along with a slow progression to the left ventricular dilation and decreased systolic function. However, the canine model shows a variable disease severity and cardiac involvement and fibrosis that only occur after several years. [48] [25] [49] [50] The hypertrophic feline muscular dystrophy model exhibits prominent hypertrophic muscle phenotype but very slight cardiac involvement. Therefore, the feline model is not translatable to the human cardiac condition. Additionally, both models are relatively large and require sophisticated and costly housing which is problematic for research use. [25] [49] [51]

1.5.3.1 Mouse models of DMD

Rodent models, specifically mice, have become popular in research due to the wide range of inbred and genetically modified strains that resemble DMD in humans. There are

numerous single-knockout and double-knockout DMD strains, such as knockouts of dystrophin alone (*mdx*), or in combination with utrophin (*mdx:utrn*$^{-/-}$), α 7-integrin (*mdx:itga7*$^{-/-}$), MyoD (*mdx:myod*$^{-/-}$), desmin (*mdx:des*$^{-/-}$), dystrobrevin (*mdx:adbn*$^{-/-}$),and parvalbumin (*mdx:pv*$^{-/-}$).[25 52 53]

By far, *mdx* mouse is the most widely DMD model. Similar to DMD patients, the *mdx* mouse has a nonsense mutation in the X-chromosome dystrophin gene which results in halting the synthesis of the dystrophin protein. Hence, the *mdx* mice are greatly applicable in skeletal muscle research. However, strain's applicability for DMD cardiomyopathy research is limited, since the *mdx* model exhibits mild and non-progressive cardiomyopathy only after 10 months of age. The mild phenotype of *mdx* mice may be due to the upregulation of the protein utrophin, which is the dystrophin homolog. Utrophin structurally substitutes and partially compensates for dystrophin in the DAPC in mice, but not in humans.[53 54 55]

In contrast, the *mdx:utrn*$^{-/-}$ mouse model, which is deficient in both dystrophin and utrophin production, demonstrates severe skeletal muscle degeneration along with cardiac dysfunction which phenocopies the human condition. These mice also exhibit abnormal gait, hind limb weakness, kyphosis, abnormal ECG and respiratory failure. They generally fail to survive after 20 weeks of age. The development of cardiomyopathy in these mice has been mapped using different imaging modalities such as 3D ultrasound and computed tomography (CT) perfusion. [25 56 57 58 59]

1.6 Imaging Modalities for detecting DCM

Diagnosis of cardiomyopathy in DMD is difficult since the patients have reduced exercise tolerance that masks the cardiac problem. DMD patients suffer from immobility, pulmonary failure, and scoliosis, which obscures the clinical and radiographic symptoms of heart failure. [37] [60] Clinically, cardiac involvement is mainly diagnosed at later stages through electrocardiography and echocardiography and sometimes detected by cardiac magnetic resonance imaging (MRI), computed tomography (CT) and radionuclide imaging.[61] [62] [63] [64]

1.6.1 Electrocardiography and Echocardiography

Electrocardiography (ECG) and echocardiography are common clinical imaging tools used to identify the structural and functional cardiac changes. ECG analyzes the electrical activity within the heart while echocardiography assesses cardiac function by ultrasound imaging. It is frequently used to elucidate changes in heart shape and size, along with the excess fluid characteristics (pulmonary congestion, pleural effusion). ECG detects left ventricular hypertrophy and cardiac arrhythmias that indicate the onset of cardiomyopathies that can lead to heart failure.[26] [65]

Echocardiography is also a powerful diagnostic tool that gives information about the ventricular size and valvular abnormalities. It enables clinicians to diagnose cardiomyopathy by measuring cardiac systolic function by ejection fraction (EF) which represents the fraction of blood pumped out of the ventricle with each heartbeat. [37] [62] [66] [67] Both techniques are relatively cost-effective and widely used in clinics. However, they provide information on structural changes that occur in the later stages of heart disease,

when the patient is experiencing outward symptoms. Additionally, echocardiography requires professional acquisition and images might be variable based on the observant expertise.[65] [61] [68]

1.6.2 Cardiac MRI and CT

Cardiac MRI detects early structural changes in DCM. It reveals three-dimensional information regarding heart size, the thickness of the ventricular wall, and function information such as ejection fraction, blood flow, fibrosis, edema, hemorrhage and changes in soft tissue. MRI is an invaluable tool which is used to diagnose and evaluate cardiac muscle abnormalities at an early stage in a non-invasive manner without exposure to radioactivity. In the clinic, gadolinium contrast-enhanced MRI aids in identifying areas of myocardial fibrosis. However, it cannot detect the diffuse fibrosis which is notable in DMD cardiomyopathy. Also, MRI for DMD patients may be limited, as many patients bear assistive implanted devices as mobility aids, which are not compatible with MRI.[69] [70] [71]

CT is another imaging modality which yields three-dimensional high resolution anatomic and morphologic information. Image contrast is dependent on the degree of x-ray attenuation by different tissues and can be enhanced by the injection of barium or iodine-based contrast agents. Contrast-enhanced CT has extremely high resolution and is excellent for imaging blood vessels, especially coronary arteries. Contrast agents are also used for coronary angiography to visualize arterial stenosis. Another type of CT, CT perfusion, measures myocardial blood flow and blood volume. The main concern to use the contrast-enhanced CT is the risk of radiation exposing the children with DMD. As the acceptable

radiation dosage for the DMD children has not been determined. The contrast agent may also cause an allergic reaction. [72 73 74]

To date, all standard diagnostic imaging tools for the detection of DMD cardiomyopathy yields information on structural changes in the heart. What is missing are indicators of the progression of heart disease at a molecular level, which can potentially detect the onset of cardiomyopathy at earlier or subclinical stages. [25] Therefore, from a clinical point of view, there is a critical need for tissue biomarkers that can identify the different stages of cardiomyopathy and predict the response to the therapy.

1.7 Biomarkers for DCM

Biomarkers are measurable indicators of biological conditions and may potentially identify the molecular mechanisms at different stages of cardiomyopathy progression. Ideally, a cardiac biomarker should comprise qualities such as: 1. Provide accurate and repeatable measurements; 2. Be present at early stages of cardiomyopathy pathogenesis; 3. Be highly sensitive to sub-clinical cardiac changes; 4. Be Cardiac-localized and 5. Be Metabolically stable and not be degraded. [69 71 75] Currently, natriuretic peptides and cardiac troponins are clinically used as biomarkers for DMD cardiomyopathy.[60 76] Specifically, elevated levels of circulating brain natriuretic peptide (also known as B-type natriuretic peptide, BNP), N-terminal pro-BNP (NT-pro-BNP) and cardiac troponins I & T indicate cardiomyocyte stress and injury and are used as a diagnostic tool for HF and DCM patients.

The hormone BNP, along with NT-pro-BNP, is secreted by ventricular cardiomyocytes upon increased wall stretching, and pressure overload as occurs in DCM. Both BNP and NT-proBNP are produced by the post-translational processing of proBNP, and N-terminal

pro-BNP is more stable than BNP in plasma. Plasma BNP levels of more than 100 pg/mL and NT-pro-BNP levels of more than 900 pg/mL are indicators of heart dysfunction. [77] [78] While BNP is commonly used as a diagnostic tool in the clinic, there are several limitations to its use as a biomarker for cardiomyopathy. First, BNP is a biomarker for severely depressed Left Ventricular Ejection Fraction (LVEF) but not for early-stage dysfunction in the left ventricle. Therefore, it cannot determine early stages of the cardiomyopathy.[78] [79] Second, there are other non-cardiac factors that affect circulating levels of BNP such as obesity and renal failure .[80] [81] Both BNP and NT-pro-BNP are also elevated in the plasma with age. These results suggest that elevated BNP levels may not be specifically due to cardiomyopathy and may vary depending on disease severity and genetic polymorphism.

The other biomarker is troponin that is a regulatory protein and present in the myofibers of striated muscles. It comprises three subunits that are products of different genes: C, I and T. Troponin C is not specific to cardiac muscle and it is not used in the clinic since its isoform is shared by skeletal muscle. Cardiac troponin I and cardiac troponin T are biomarkers of cardiac stress and historically used to diagnose myocardial infarction. While increases in circulating levels of both cardiac troponins I and T are associated with myocardial necrosis and remodeling, the assay for troponin I assay is the most sensitive and specific test in the clinic.[82] In DMD, increased cardiomyocyte sarcolemma permeability and stretching leads to the release of troponins from the cytosolic pool. Furthermore, an increase in cardiac ventricular wall stress causes cardiomyocyte apoptosis and disruption of the contractile force resulting in troponin release. However, cardiac troponins are also elevated in other cardiovascular diseases such as hypertrophic

cardiomyopathy, hypertension, myocarditis and cardiac amyloidosis and only provide information at the late stages of DMD cardiomyopathy. [75 83 84]

Although both circulating biomarkers are detectable by a simple blood test, they are not specific to the heart and may be produced by other tissues in response to injury. Moreover, circulating levels might not be representative of those found within the cardiac tissue. Therefore, it is necessary to identify cardiac- localized biomarkers for DMD cardiomyopathy. [68]

One possible biomarker is the cardiac-localized is the growth hormone secretagogue receptor (GHSR) and its ligand, ghrelin. I will now elaborate on the ghrelin/GHSR system as a cardiomyopathy biomarker.

1.7.1 GHSR and ghrelin: general physiology

Ghrelin and its receptor, GHSR, represent a potential candidate biomarker for cardiomyopathy. Ghrelin is a 28 amino-acid peptide hormone and is the natural ligand of GHSR, a seven-transmembrane, G protein-coupled receptor. This peptide hormone plays an important role in systemic metabolism by appetite stimulation and food intake regulation. Ghrelin levels in plasma are raised in the fasted state and reduced after a meal.[85]

Mature bioactive ghrelin is produced from the post-translational cleavage of pro-ghrelin (117 amino-acid) and is octanoylated on serine 3 by ghrelin O-Acyltransferase (GOAT), which enables binding to GHSR. The proportion of ghrelin that does not bear this modification is termed des-acyl ghrelin and does not bind to GHSR.[86]

Molecular features of ghrelin are located in N-terminal region, particularly in residues 1-8 of the peptide which is required for activation of GHSR.[87] The binding of ghrelin to GHSR induces signaling through $G\alpha_{q11}$ which results in growth hormone release.[88]

Ghrelin was originally isolated from rat and human stomachs, but it is also synthesized in and secreted from other tissues including those of the cardiovascular system.[85 89] Specific binding of ghrelin in cardiovascular tissues such as myocardium, aorta, coronary arteries, pulmonary arteries and veins has been reported, demonstrating that GHSR is expressed throughout the cardiovascular system.[90]

1.7.1.1 Ghrelin & GHSR in the Cardiovascular System

The expression of myocardial GHSR and the production of ghrelin from cardiomyocytes and vascular endothelial cells suggests the presence of ghrelin/GHSR system in the heart that operates independently of its function in the regulation of appetite.[89] One study has shown that ghrelin had effects on the cardiovascular system through GHSR in GH-deficient rats, further demonstrating the independence of the cardiovascular ghrelin/GHSR system[91 92] As well, ghrelin synthesis by the myocardium and cultured cardiomyocytes suggests that ghrelin could have autocrine and paracrine effects in cardiac muscle.[93 94]

The binding of GHSR by ghrelin activates numerous signaling pathways that mediate the cardiovascular effects of ghrelin.[95] At the level of the cardiomyocyte, these effects include the promotion of contractile activity, stimulation of angiogenesis and proliferation, and inhibition of apoptosis.[91]

Activation of GHSR by ghrelin results in subsequent activation of phospholipase C (PLC), which cleaves phosphatidylinositol 4,5-bisphosphate (PIP_2) into IP_3 and diacylglycerol.

Diacylglycerol binds to and activates PKC, which then activates L-type voltage-dependent Ca^{2+} channels in the sarcolemma, and IP_3 facilitates calcium release from the sarcoplasmic reticulum (SR), which is necessary for cardiomyocyte contraction.[95] The binding of ghrelin to myocardial GHSR also activates other molecular pathways such as PI3K and AKT that promote angiogenesis, cell proliferation and migration.[96] Signaling through PI3K and ERK1/2 is also associated with inhibiting apoptosis. Ghrelin inhibits apoptosis induced by doxorubicin in cardiomyocytes by elevation of the antiapoptotic factors IGF-1 and cardiotrophin-1 (CT-1). Therefore, ghrelin activation of GHSR in cardiomyocytes promotes contractile activity and survival and inhibits apoptosis.[97]

Several studies conducted in various animal models of heart disease provide evidence for the cardioprotective effects of the ghrelin/GHSR system and its potential for diagnosis and treatment of cardiovascular diseases. Administration of ghrelin in an ischemia-reperfusion rat model decreased infarct size and improved left ventricular function. [91] [98] Ghrelin also attenuated left ventricular remodeling in rats after myocardial infarction as well as in obese mice.[99] [100] In animal models of HF, ghrelin administration improved myocardial contractility and reduced cachexia.[101]

In humans, ghrelin administration also improved cardiac output in patients with congestive HF, suggesting that ghrelin may have a therapeutic role in HF.[89] In healthy humans, intravenous ghrelin injection improved cardiac output and contractility and reduced arterial pressure with no changes in heart rate.[102] Nagaya et al. reported that ghrelin administration improved left ventricular function by attenuating left ventricular remodeling in chronic HF patients. They also showed that ghrelin administration reduced the vascular resistance and improved the stroke index and cardiac output in chronic HF patients.[103] They also observed

that ghrelin treatment boosted the lean body mass, muscle strength, and oxygen consumption during exercise, suggesting that ghrelin may reduce the extent of muscle wasting in chronic HF patients.[103]

Ghrelin action in the vasculature and particularly endothelial cells is complex due to the activation of different pathways. Ghrelin binding to GHSR on endothelial cells promotes NO synthesis through activation of PI3K/AKT and eNOS signaling pathways.[104] Tesauro et al. showed that ghrelin could reverse endothelial cell dysfunction in metabolic syndrome patients through an increase in NO bioavailability, thereby suggesting a role for ghrelin in vascular hemostasis [105]. Signaling through the PI3K/AKT pathway also leads to protection of endothelial cells against oxidative stress and apoptosis.[95] [106]

1.7.1.2 Ghrelin & GHSR in Inflammation

Ghrelin may have an anti-inflammatory role in the immune and vascular system. Studies have demonstrated that levels of GHSR are increased in acute vascular inflammation. Human coronary endothelial cells and smooth muscle cells incubated with lipopolysaccharide to induce inflammation showed increased GHSR mRNA levels, and inflammation was attenuated after treatment of the cells with ghrelin. [107] Ghrelin also hindered the production of the pro-inflammatory cytokine IL-8 and NF-κB signaling activation in human umbilical vein endothelial cells (HUVECs) treated with TNF-α.[108]

Ghrelin also has direct anti-inflammatory effects on immune cells. It has been shown that GHSR is expressed in human monocytes and T-cells, and treatment with ghrelin blocks the

secretion of the pro-inflammatory cytokines IL-1, IL-6 and TNF-α. [109] *In vivo*, treatment of a rat model of arthritis with a ghrelin analog for eight days attenuated the level of inflammation by reducing the plasma concentration of cytokines.[110]

The anti-inflammatory effect of ghrelin has also been reported in acute myocardial inflammation. Ghrelin injection ameliorated the inflammatory post-infarction myocardial remodeling in rats induced by coronary artery ligation. Subcutaneous injection of ghrelin decreased the left ventricular remodeling and scar thickness and inhibited the inflammatory response as determined by reductions in mRNA and protein levels of IL-1 and TNF-α. [111] Since ghrelin appears to have cardioprotective and anti-inflammatory effects on cardiomyocytes and vascular endothelial cells through GHSR, we need to have more insight into patterns of GHSR changes in cardiomyopathy. Since DMD dilated cardiomyopathy is a combination of inflammation, ischemia and fibrosis, elucidating the relationship between inflammation and GHSR in this condition could provide more insights into the progression of dilated cardiomyopathy.

1.7.1.3 Our GHSR strategy

Our collaborative research group has developed and characterized novel fluorescent tools for the detection of GHSR *in situ.* In particular, we have generated peptide analogs of ghrelin and des-acyl ghrelin conjugated to the far-red fluorophore, Cy5: Cy5-ghrelin (1-19) and Cy5-des-acyl ghrelin (1-19). Using these tools, our previous work demonstrated that only the octanoylated form of ghrelin bound to GHSR in murine cardiomyocytes[112]. With the Cy5-ghrelin(1-19) probe we were also able to track the differentiation of P19 cells into cardiomyocytes, demonstrating that we can follow changes in GHSR over time.[112]

Using Cy5-ghrelin (1-19), our lab showed that levels of cardiac GHSR decreased in a mouse model of diabetic cardiomyopathy which represented early-stage DCM[113], and investigated the dynamics of GHSR before and after cardiac transplantation in humans with end-stage HF. In this important study, we also found an inverse correlation between LVEF and myocardial GHSR levels and demonstrated that GHSR may be more sensitive than BNP as a cardiac-localized biomarker for HF. [114]

Overall, our lab has identified the GHSR/ghrelin system as a possible cardiac-localized biomarker for human end-stage HF and the early stages of murine diabetic cardiomyopathy. These findings led to my study investigating if GHSR is a biomarker in the highly inflammatory and fibrotic cardiomyopathy of DMD.

1.8 Central Hypothesis

My studies focused on characterizing changes in GHSR, ghrelin and inflammatory markers in the heart and cardiac microvasculature, in a mouse model of DMD cardiomyopathy.

Hypothesis: I hypothesize that GHSR levels positively correlate with the severity of cardiac and vascular inflammation in DMD

The aims of this project are:

1. To characterize GHSR and inflammatory markers in late-stage cardiomyopathy in a mouse model of DMD
2. To characterize GHSR in mouse vascular endothelial cells and its correlation with levels of induced inflammation

Chapter 2

2 Material and Methods

2.1 Animal models

Experiments were performed at The Lawson Health Research Institute at St. Joseph's hospital in London, Ontario. All animal protocols were approved (Ethics approval #2008-067) by the Western University Institutional Animal Use Subcommittee and conducted according to guidelines set by the Canadian Council on Animal Care (CCAC).

2.1.1 Wild type (C57BL/6 Mice)

As a negative control, wild-type C57BL/6 mice were purchased from Charles River Laboratories (Wilmington, MA, USA) at the age of 4-5 weeks and housed at the Lawson Health Research Institute Animal Care Facility. Mice were maintained in controlled conditions (19-23˚C, 12-hour light/dark cycles), fed regular mouse chow and monitored daily to ensure their health. Food and water were provided *ad libitum*.

2.1.2 Heterozygous *mdx* mice (*mdx:utrn*$^{+/-}$)

Heterozygous *mdx* mice (*mdx:utrn*$^{+/-}$) were generously provided by Dr. Robert Grange, Virginia Polytechnic Institute and State University, Blacksburg, VA, USA. This strain was originally generated by Dr. Mark Grady and Dr. Joshua Sanes from Washington University, St. Louis, MO, USA. Heterozygous utrophin *mdx* mice (*mdx:utrn*$^{+/-}$) have an intermediate disease phenotype compared to the double knockout mice.[115]

2.1.3 Mouse model of DMD mice (*mdx:utrn*$^{-/-}$)

Heterozygous *mdx* mice were crossed to generate *mdx:utrn*$^{-/-}$mice which lack both utrophin and dystrophin. Only male groups of wild-type and *mdx:utrn*$^{-/-}$ mice at the age of 15-17 weeks were used in this study. At this age range, *mdx:utrn*$^{-/-}$ mice demonstrate the severe phenotype of DMD disease [53] and do not tend to live past 20 weeks of age. In this thesis, the DMD mouse refers exclusively to the *mdx:utrn*$^{-/-}$ mouse.

2.2 Animal genotype validation

For genotyping, tail snips or ear-notches were collected, and DNA was extracted according to the standard PCR genotyping protocol. Briefly, tail snips or ear-notches were lysed using Proteinase K at 55° C overnight. Then, the polymerase chain reaction (PCR) was performed by Taq polymerase enzyme (Biolabs, M0267E) to amplify the utrophin gene.[52]

The set of primers that were used to confirm the presence of utrophin were:

5'- TGCCAAGTTCTAATTCCATCAGAAGCTG -3' (forward primers)

and 5'- CTGAGTCAAACAGCTTGGAAGCCTCC-3' (reverse primer)

Gene deletion was confirmed by the existence of a band at 310 kb on a 1% agarose gel containing ethidium bromide.

2.3 Heart sample preparation

All hearts were obtained from mice from a previous study in which cardiomyopathy had been measured by determining left ventricular ejection fraction through micro-CT and 3D echocardiography.[59] In that study, the hearts from each of three 15-17 week-old WT and three *mdx:utrn*$^{-/-}$ mice were removed immediately after CO_2 euthanasia, and fixed in 10% buffered formalin for 48 hours[116]. Then, they were cut axially into two equal sections and embedded in paraffin. Tissue processing and sectioning were done by the Pathology Core Facility at Robarts Research Institute (Western University, London, Ontario).

2.4 Tissue Sectioning

Tissue blocks were sliced in 5μm serial sections with a total of 40 sections for each block of cardiac tissue. To ensure that sections were representative of the whole cardiac tissue, serial sections were taken every 10 slices for histological analysis and fluorescent staining. The selected tissue sections (5 per heart) were deparaffinized and dehydrated with a series of xylene, 100%, 90% and 70% ethanol prior to staining.[116]

2.5 Histological imaging

2.5.1 Image acquisition

Hematoxylin and Eosin (H&E) and Masson's Trichrome staining was performed by the Pathology Core Facility at Robarts to qualitatively assess tissue architecture and the level of fibrosis, respectively. Images were acquired on a Zeiss Axioscope microscope with Northern Eclipse software v7.0 (Empix Imaging Inc) under 10x, 20x and 40x objectives. Non-overlapping fields of view were taken to image the entire tissue for each section

with the 10x objective. As well, the entire tissue section was raster scanned at 10x to provide an unbiased view of the staining. To have more insight for each section, 6 fields of view were taken with the 20x and 40x objectives.

2.6 Immunostaining

For immunostaining, heat-mediated antigen retrieval was performed with 10 mM sodium citrate buffer in Phosphate Buffered Saline (PBS), pH =7.4, for 20 minutes prior to staining.[116] Then, tissues were incubated with blocking buffer (10% Donkey serum (Sigma-Aldrich, D9663) + 1% bovine serum albumin (BSA) in PBS) for 1 hour at room temperature. Slides were then incubated with primary antibodies (antibodies are listed in Table 1 and described in Section 2.6.2) overnight at 4° C followed by incubation with secondary antibodies (listed in Table 1 and section 2.6.2) for 2 hours at room temperature. Finally, Cy5-ghrelin (1-19) (1:100) or Cy3-des-acyl-ghrelin (1-19) (1:100) were added to slides and incubated for 30 minutes.

2.6.1 Designing of fluorescent ghrelin analogs

The fluorescent ghrelin analogs, Cy5-ghrelin (1-19) and Cy3-des-acyl-ghrelin (1-19), were used to detect GHSR and des-acyl-ghrelin binding, respectively, in the cardiac tissues. These probes were synthesized as described previously[112]. Structures are illustrated in Figure 2.

A B

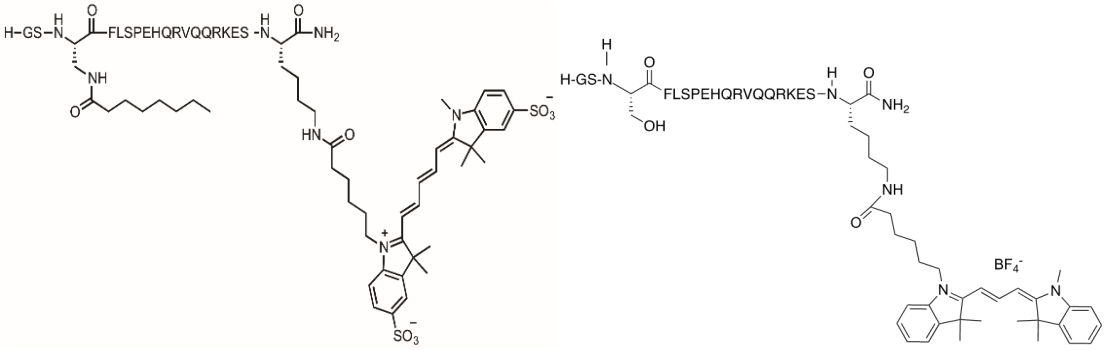

Figure 2. Structure of ghrelin probes. A) Structure of Cy5-ghrelin (1–19); (Dpr3(octanoyl), Lys19(Cy5) B) Structure of Cy3-des-acyl-ghrelin (1–19).

2.6.2 Antibodies

A) F4-80: For immunofluorescent detection of macrophages, rat monoclonal anti-F4-80 antibody (1:200, Abcam, ab16911) was used and visualized with Alexa Fluor-594 conjugated donkey anti-rat IgG (1:500, Life Technologies, A21209). This antibody targets the F4-80 antigen (glycoprotein) that is expressed by murine macrophages.

B) IL-6: To demonstrate the acute phase of the inflammatory response, mouse monoclonal anti-IL-6 (1:100, Abcam, ab9324) was used, followed by Alexa Fluor-594 conjugated donkey anti-mouse IgG (1:500, Life Technologies, A21203) for visualization. This antibody targets the IL-6 cytokine which is produced by cardiomyocytes, macrophages and adipose tissue.

C) Isolectin Conjugate: Isolectin GS-IB4 Alexa Fluor 488 Conjugate (1:100 Life Technologies, I21411) was used to stain the endothelial cells. This conjugate is composed of the Isolectin IB_4 glycoprotein which is a part of the five tetrameric lectin family and targets α-D-galactosyl residues on cell membranes. This conjugate labels the endothelial cells which are in the inner wall of the vasculature (microvasculature and macrovasculature), and also labels murine macrophages and laminin.

D) CD36: Rabbit Polyclonal anti-CD36 antibody (1:250, Novus Biologicals, NB400-144) was used along with using Alexa Fluor-594 conjugated donkey anti-rabbit IgG (1:500, Life Technologies, A21206). This antibody marks the leukocyte differentiation antigen, CD36 which is found in the tissues that are involved in lipid metabolism such as adipocytes, microvascular endothelial cells and cardiomyocytes.

E) Nuclei were visualized with DAPI Prolong Diamond mountant (Thermo Fisher Scientific, P36962).

To capture the background autofluorescent staining in the images, tissue sections were incubated only with the secondary antibodies (Alexa Fluor-594 conjugated donkey anti-rabbit IgG, Fluor-594 conjugated donkey anti-mouse IgG, Alexa Fluor-594 conjugated donkey anti-rat IgG and Alexa Fluor-488 conjugated donkey-anti-mouse IgG).

2.6.3 Confocal Microscopy

2.6.3.1 Image acquisition

Sections were imaged on a confocal microscope (Nikon A1 R Canada) equipped with NIS Elements AIR 5.02.00 software using a 60x oil-immersion objective. The microscope was equipped with four lasers: DAPI (405nm), FITC (490nm-519nm), TRITC (561nm-594nm) and Cy5 (633-647nm), and they were switched on separately to reduce the cross-talk between the fluorochromes. Five sections were imaged per cardiac tissue and for each section, five regions of interest (ROIs) were captured. To visualize the microvasculature, the Nyquist option of image capturing was used to capture the field of interest and then image acquisition was done by higher pixel resolution (1024). To visualize the large vessels, five sections were imaged per cardiac tissue, and ten ROIs within the vessel structure were captured. To display the maximum contrast and brightness, images were deconvoluted using the 2D deconvolution algorithm on NIS Elements AIR 5.02.00.

2.6.3.2 Image analysis

The analysis was done using the ROI statistic option of the NIS Elements AIR 5.02.00 software.

A) Fluorescence intensity analysis was conducted on the 5 ROIs from each section and the intensity was normalized to the negative control (secondary antibody alone) as described above. The fluorescence intensity analysis was done for Cy5-ghrelin (1-19), Cy3-des-acyl-ghrelin (1-19), F4-80, IL-6 and CD36.

B) The extent of colocalization was determined by using the colocalization analysis in NIS Elements. This software generates a scatter plot of red and green (representative of CD36 and isolectin), green and purple (representative of Isolectin and GHSR), purple and red (representative of GHSR and IL-6, GHSR and F4-80)

were used to determine the levels of correlation between each pair of markers. Then, by using Coste's algorithm the Pearson's correlation coefficient (PCC) was computed.

2.6.3.3 Statistical Analyses

Statistical analyses were conducted, and graphs were plotted using GraphPad Prism v.7.03 (San Diego, California, United States). T-Test was used to compare the levels of GHSR between the DMD and age-matched WT using SPSS software v.24.0. A p value of <0.05 was considered significant. To correlate the level of inflammation with GHSR, linear regression analysis was run on the F4-80 vs. GHSR data and also on IL-6 vs. GHSR data.

2.7 Cell Culture

For mechanistic studies, mouse cardiac microvascular endothelial cells (MCEC) were purchased from Cedarlane (Burlington, Ontario, Canada). The MCECs were maintained in Dulbecco's Modified Eagle Medium (DMEM) (Life Technologies, 11960-044) supplemented with 5% Newborn Calf Serum (NCBS) (Life Technologies, 16010142), 2 mM L-glutamine (Life Technologies, 25030081) and 100 units/mL penicillin-streptomycin (Life Technologies, 15070063), at 37°C and 5% CO_2. When MCECs reached 75-90% confluency they were dissociated from the plate with 0.25% trypsin/EDTA (Thermo Fisher Scientific,25200072) for 5 minutes at 37°C and 5% CO_2 and then diluted in regular supplemented DMEM. The collected cells were seeded in 100-mm dishes for western blotting or on 60-mm tissue culture dishes containing glass coverslips for

immunocytochemistry studies. Treatment with 10 ng/mL, 250 ng/mL and 500 ng/mL of TNF-α (Abcam, ab9740) or vehicle control was performed in serum-free DMEM for 6, 16 and 24 hours.[117]

2.8 Immunocytochemistry and Immunofluorescence Microscopy

2.8.1 Immunostaining

At the end of each treatment, cells were fixed with 2% paraformaldehyde (PFA) (Electron Microscopy Sciences, 15710-S) for 30 minutes at room temperature, permeabilized with 0.25% Triton-X100 for 5 minutes and blocked with 1% bovine serum albumin (BSA) (Fisher Scientific, BP6711) in PBS for 1 hour at room temperature. The coverslips were incubated with the primary antibody, mouse anti-ICAM-1 (Intercellular Adhesion Molecule 1, 1:250, Abcam, ab171123), overnight at 4°C. Mouse anti-ICAM-1 targets the glycoprotein on the cell surface of the endothelial cells. Upon cytokine stimulation, the level of ICAM-1 increases in the endothelial cells.

To visualize ICAM-1, cells were incubated with the secondary antibodies, Alexa Fluor-488 conjugated donkey anti-mouse IgG (1:500), for 2 hours at room temperature. Then, cells were incubated with Cy5-ghrelin (1-19) (1:100) for 30 minutes to visualize GHSR. Coverslips were mounted using the Prolong Diamond mountants with DAPI (Thermo Fisher Scientific, P36962). As a negative control, cells were incubated with the secondary antibodies alone.

2.8.2 Confocal Microscopy

2.8.2.1 Image acquisition

Slides were imaged on a confocal microscope (Nikon A1 R Canada) equipped with NIS Elements AR 5.02.00 software using a 60x oil-immersion objective. The microscope was equipped with four lasers including DAPI (405nm), FITC (490nm -519nm), TRITC (561nm-594nm) and Cy5 (633-647nm) and they were switched on separately to reduce the crosstalk between the fluorochromes. Images were acquired from four slides per treatment at five regions of interest (ROIs) per slide. To display the maximum contrast and brightness in all images, the deconvolution algorithm on NIS Element AR 5.02.00 was applied in the same manner to all images.

2.8.2.2 Image analysis

The analysis was done using the ROI statistic option of the NIS Element AR 5.02.00 software as described in Section 2.6.3.3. The fluorescence intensity analyses for GHSR (Cy5-ghrelin (1-19)) and ICAM-1were conducted on the five ROIs from each slide and the intensities were normalized to their negative control. Colocalization analysis generated a scatter plot of green and red which represents the co-expression of ICAM-1 and GHSR. Coste's algorithm computed the Pearson's correlation coefficient (PCC) as stated above.

2.8.2.3 Statistical Analyses

Statistical analyses were conducted, and graphs were plotted using GraphPad Prism v.7.03 (San Diego, California, United States). One-way ANOVA used to compare the levels of

GHSR and ICAM between the treated and untreated cells with TNF-α on the means of four technical replicates. A p value of <0.05 was considered significant.

2.9 Cell lysates & Immunoblotting

2.9.1 Western blotting

Cell lysates were prepared in radioimmunoprecipitation assay (RIPA) lysis buffer (Life Technologies, 89900) containing proteinase inhibitor mini-EDTA (Sigma Aldrich, 11836153001). Protein content was quantified using a bicinchoninic acid (BCA) assay kit (BioVision, K813-2500). Thirty μg of total protein were loaded in each lane and separated on 4-12% NUPAGE gel (Invitrogen, NP0335). The resolved bands were transferred onto polyvinylidene difluoride (PVDF) membranes (Life Technologies, IB401001) using the iBlot® dry transfer system (Invitrogen). Membranes were blocked in 5% BSA in Tris-buffered saline-Tween (TBST) for 1 hour at room temperature. Then, membranes were probed with primary antibodies including rabbit anti-GHSR (1:500, Santa Cruz Biotechnology, sc-374515) and anti-beta-actin (1:1000, Abcam, ab199799) overnight at 4°C. Bands were visualized using secondary antibodies conjugated to horseradish peroxidase (HRP): goat anti-rabbit HRP (1:1000, Invitrogen, PI31460) and goat anti-mouse HRP (1:1000, Abcam, ab6789). Bands were visualized with western ECL substrate (Thermo Fisher Scientific, 32106).

2.9.2 Image acquisition and analysis

Membranes were imaged using a BioRad ChemiDoc Imaging System. Band intensities were determined by ImageJ FIJI version 1.46 (National Institute of Health, Maryland, United States) and normalized to the beta-actin band intensities. The values were statistically compared using one-way ANOVA. Densitometry units are displayed as mean ± SEM and a p-value of <0.05 was considered significant.

Table 1. Antibodies used for immunofluorescence microscopy.

Antibodies	**Source**	**Dilution**	**Target**	**Catalog**	**Research Resource Identification number**
Rat F4-80	Abcam	1:200	F4-80 glycoprotein	ab16911	AB-443548
Mouse IL-6	Abcam	1:100	IL-6 Cytokine	ab9324	AB-307175
Rabbit CD36	Novus Biologicals	1:250	CD36 antigen	NB400-144	AB-10003498
Mouse ICAM-1	Abcam	1:250	ICAM-1 glycoprotein	ab171123	
Rabbit GHSR	Santa Cruz Biotechnology	1:500	GHSR	sc-374515	AB-10987651

Rabbit Beta-actin	Abcam	1:1000	Beta-actin	Ab8227	AB-2305186
Isolectin GS-IB4 Alexa Fluor 488 Conjugate	Life Technologies	1:100	Endothelial cells	I21411	AB-2314662
Alexa Fluor-594 conjugated donkey anti-Rat IgG	Life Technologies	1:500		A21209	AB-2535795
Alexa Fluor-594 conjugated donkey anti-mouse IgG	Life Technologies	1:500		A21203	AB-141633

Chapter 3

3 Results

3.1 Characterization of cardiac tissue pathology in the DMD heart

I characterized the cardiac tissue pathology in wild-type and *dmd* (*mdx:utrn*$^{-/-}$) cardiac tissues stained with hematoxylin and eosin (H&E) and Masson's trichrome. For each slide, the entire tissue section of the myocardium in WT and DMD mice was screened to determine the full extent of degeneration and fibrosis. The left ventricular myocardium of DMD mice was mainly affected, so analysis focused on this region. We first compared the cellular organization between WT and DMD mice at 15-17 weeks of age **(Figure 3)**.

In WT mice, cardiac muscle fibers were organized and had a cross-striation that provides the three-dimensional network connected by intercalated disks (**Figure 3 panels A** and **B**). Cardiomyocytes were either mononucleated or binucleated with a central nucleus in the extensive pinkish-red cytoplasm **(Figure 3, panel C)** In contrast, cardiac myofibers in DMD mice were shrunken, had lost their nuclei and striation, and stained palely with eosin **(Figure 3 panel F)**. Vacuoles were also found within the cardiomyocyte sarcoplasm and could be a manifestation of myofiber necrosis and cardiomyopathy **(Figure 3 panel E).** Pyknotic nuclei and aggregation of lymphocytes indicate the necrosis and chronic inflammation within the myocardium of the DMD mice **(Figure 3 panel E).** Our findings illustrate that the pathology of cardio muscular dystrophy in DMD mice includes pyknosis (black arrow), lymphocytic infiltration (green arrow), vacuolization (red arrow).

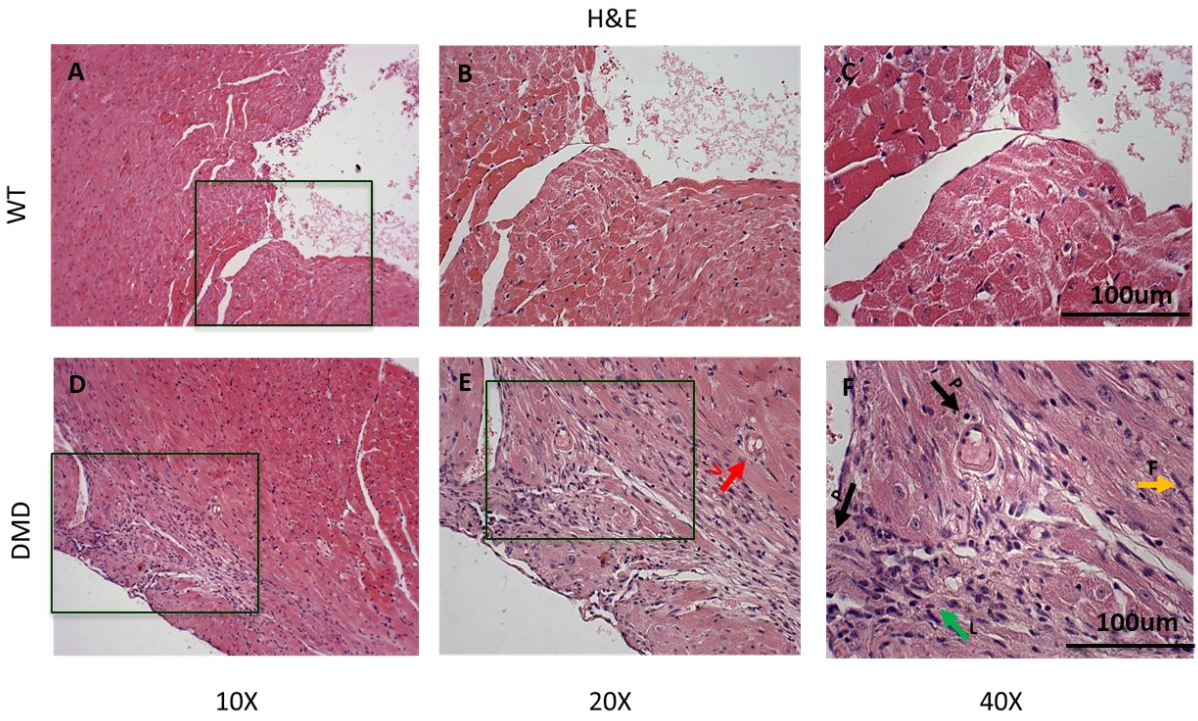

Figure 3. Representative images of cardiac tissue architecture of the left ventricle in wild-type and DMD *(mdx:utrn$^{-/-}$)* mice at 15-17 weeks of age(n=3).

Cardiac tissue sections were stained with Hematoxylin and Eosin (H&E) and images were acquired at 10x, 20x and 40x magnification of the myocardium of the left ventricle in wild-type (top row) and DMD (bottom row) mice. (B), Cardiac muscle fibers form the interconnecting three-dimensional network. (C), Cardiac muscle cells contain one or two nuclei which are centrally located with extensive eosinophilic cytoplasm; healthy cardiac fibers have regular cytoplasmic cross-striations. (E), Cardiac myofibers in DMD mice are loose without cross-striation. The red arrow indicates cardiomyocyte vacuolation that is a marker of cardiac degeneration. (F), The size of nuclei in the cardiomyocytes is variable. The black arrows show the shrunken myocyte and pyknosis in the myocardium. Yellow and green arrows indicate a fibroblast and lymphocyte aggregates, respectively. Boxes represent the magnified areas.

To determine the extents of both cardiac tissue degeneration and fibrosis simultaneously, we aligned the H & E and Masson's trichrome staining in the same area of the cardiac tissue. To determine the level of fibrosis in the wild-type and DMD mice, Masson's trichrome staining was performed to visualize the collagen content in the myocardium. The myocardium stained red while the collagen content was blue. We compared tissue morphology/architecture with the extent of fibrosis. In WT mice, cardiac myofibers in the lateral wall of the LV were uniformly red, organized and didn't have any collagen staining **(Figure 4, bottom row)**. In contrast, there was a significant amount of fibrosis in the lateral wall of the left ventricle in DMD mice **(Figure 5, panel D)**. There were pyknotic nuclei and lymphocyte infiltration above the collagen fibers **(Figure 5, panels C and F)**. Fibroblasts, which are the elongated (spindle-shaped) cells, were located adjacent to the collagen fibers **(Figure 5, panel F)**.

I also investigated the extent of fibrosis in the LV apex of DMD mice **(Figure 6).** At 10X magnification, the loss of organized architecture of myofibers was visualized, and there was a large extent of collagen and fat deposition in this area **(Figure 6, panels A and D).** At a higher magnification, pyknotic nuclei and aggregation of lymphocytes were seen **(Figure 6, panels C and F)**, indicating cardiomyocyte necrosis and chronic inflammation, respectively. There are also large areas of adipose tissue and collagen deposition in the LV apex of the DMD myocardium that surround disorganized and degenerated myofibers (**Figure 6, panel F**).

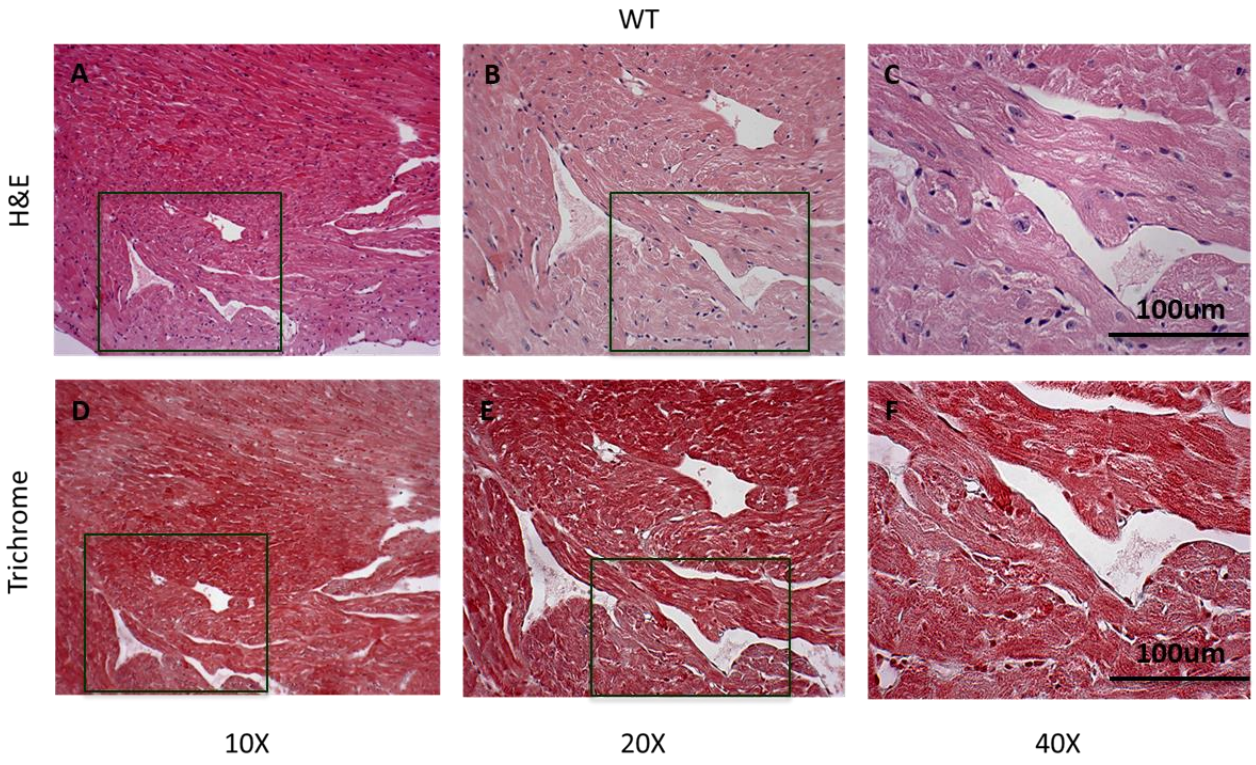

Figure 4. Representative histology images of the left ventricle in wild-type cardiac tissue (n=3). Architecture of the heart in WT mice with 10x, 20x and 40x magnifications. (A, B, C) H&E staining of left ventricle myocardium in WT mice. Myocardial fibers are organized and have normal striation. The cardiomyocytes are either mononucleated or binucleated which are blue in color and centrally located. (D, E, F) Masson's Trichrome staining of left ventricle myocardium in wild-type mice. The cardiac muscle is bright red and there is no collagen content (blue staining) in the wild-type myocardium. (Boxes represent the magnified area)

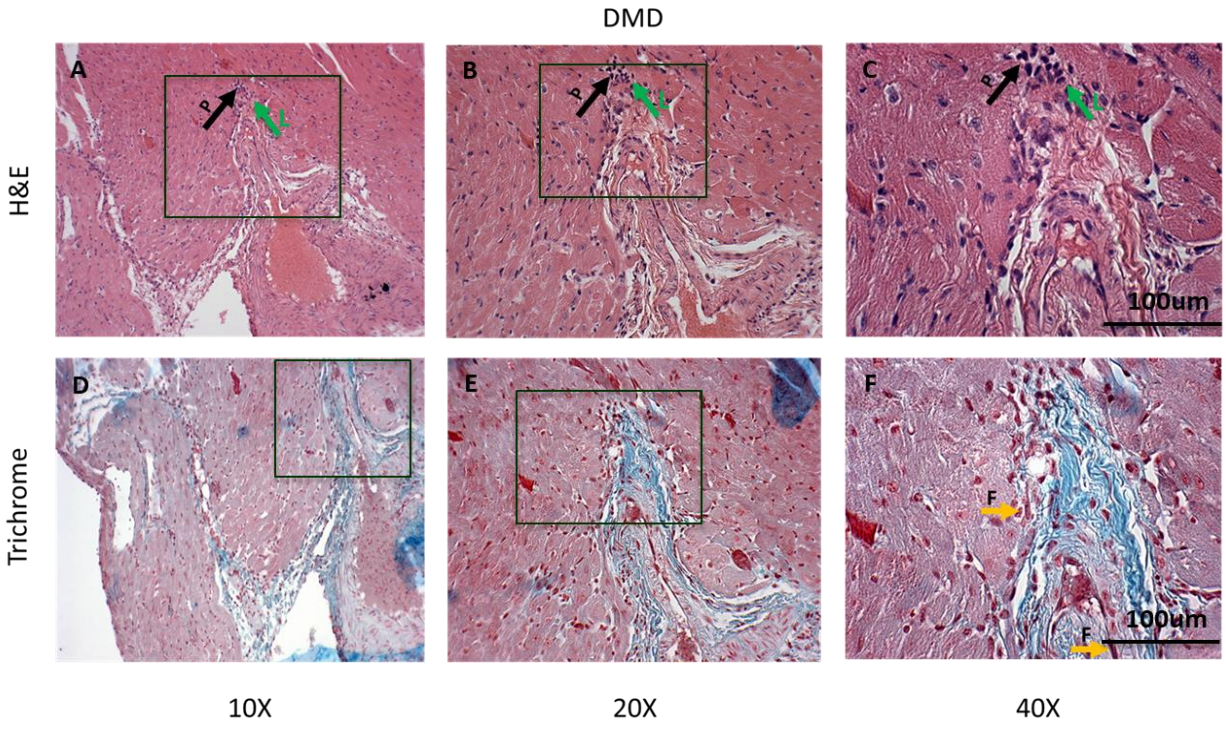

Figure 5. Representative histology images of the left ventricle in DMD (*mdx:utrn*$^{-/-}$) mice (n=3). (A, B, C) H&E staining at 10x, 20x and 40x magnification, respectively. Myocardial fibers are disorganized and have irregular striation. The cardiomyocytes' nuclei are acentric and variable in size. The black arrow indicates an area of pyknotic nuclei, and the green arrow points to lymphocytes. (D, E, F) Masson's trichrome staining; the panels align with the H&E staining above. (D), The diffuse pattern of collagen deposition in the DMD heart. (E), Cardiac myofibers show a loss of striation around an area of collagen deposition. (F), The size of nuclei in the cardiomyocytes is variable. The yellow arrows indicate fibroblasts adjacent to the area of collagen deposition. Boxes represent the magnified areas. Panels A and D are not completely aligned due to the blue artifacts in Masson's Trichrome staining.

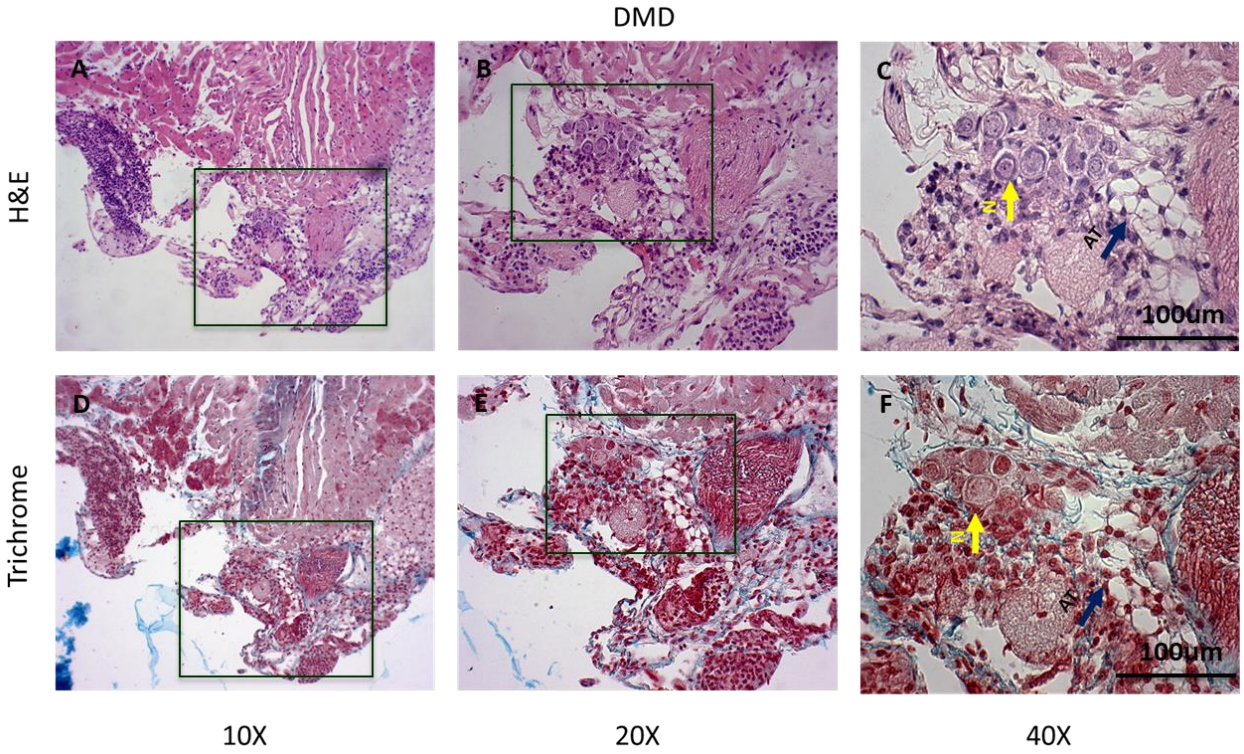

Figure 6. Representative histology images of the left ventricular apex in DMD (*mdx:utrn*$^{-/-}$) mice(n=3). (A, B, C) H&E staining at 10x, 20x and 40x magnification, respectively. High magnification in panel C reveals the disruption in myocardial tissue organization, leukocyte infiltration, adipose tissue deposition (blue arrow) and neurons (yellow arrow). (D, E, F) Masson's trichrome staining. These panels align with the H&E staining above. (E) There is diffuse fibrosis (blue) and cardiac tissue stains pale red. (F) The blue arrow indicates the adipose tissue in the myocardium and the adjacent myofibers are degenerated. (F) Yellow and blue arrows indicate neurons and adipose tissue, respectively. Boxes represent the magnified areas.

3.2 GHSR in cardiac tissue

Our lab has previously shown that GHSR may be a biomarker of heart failure in humans [114] and also a biomarker of diabetic cardiomyopathy in mice [113]. The next set of experiments investigated if GHSR was present in the microvasculature of the heart, and how GHSR levels are altered with levels of inflammation during the progression of dilated cardiomyopathy in DMD mice.

I stained the cardiac tissues with Cy5-ghrelin (1-19) along with AlexaFluor488-isolectin to evaluate the presence of GHSR in the microvasculature within the myocardium of WT and DMD mice. GHSR is present at very low levels in WT cardiomyocytes and is significantly elevated ($p<0.0001$) in DMD heart (**Figure 7A** and **B**). Microvessels in the myocardium of WT demonstrated an organized and cylindrical shape. The expression of GHSR was not seen in the microvessels since there was no colocalization between the isolectin and Cy5-ghrelin (1-19) binding (**Figure 7A**). In DMD mice, the cylindrical architecture of the microvessels in the left ventricle appeared to be disrupted, and there was also no colocalization between isolectin and Cy5-ghrelin (1-19) (**Figure7A**). Therefore, GHSR does not appear to be present in the cardiac microvasculature in either WT or DMD mice.

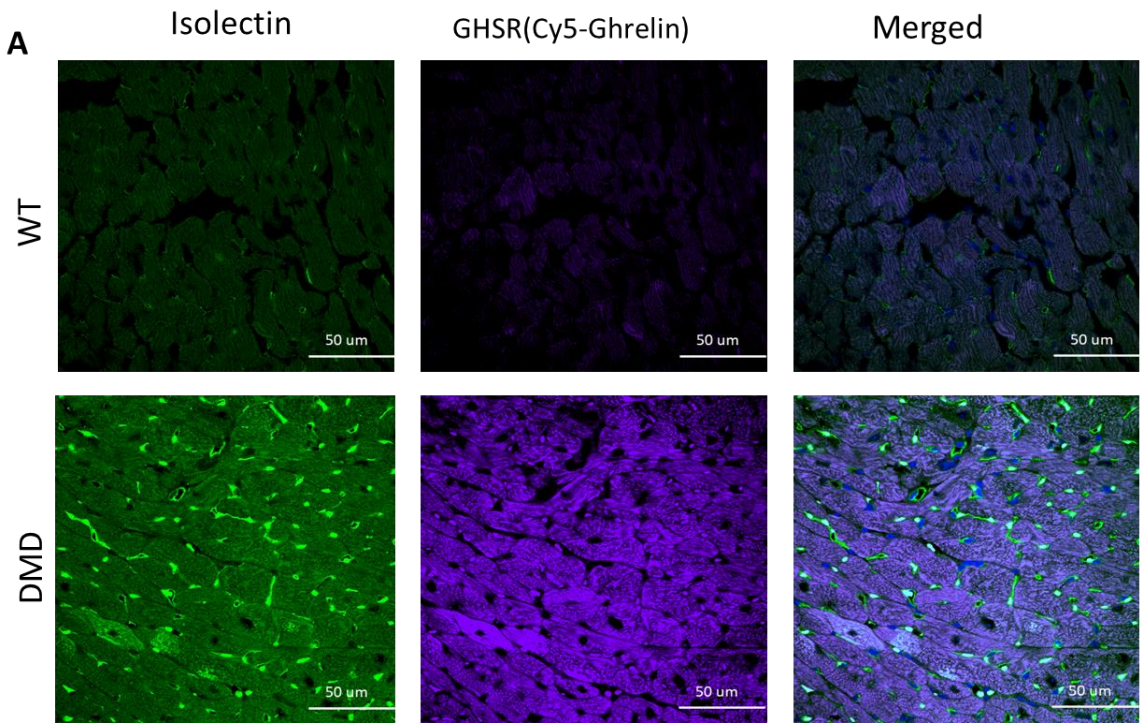
A
Isolectin
GHSR(Cy5-Ghrelin)
Merged
WT
DMD
50 um

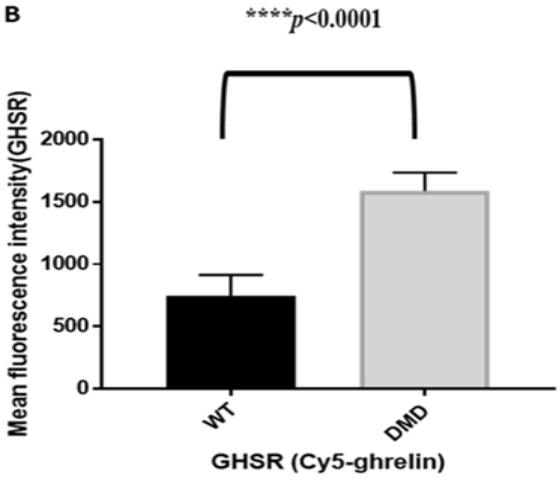
B
****p<0.0001
Mean fluorescence intensity(GHSR)
2000
1500
1000
500
0
WT
DMD
GHSR (Cy5-ghrelin)

Figure 7. GHSR expression is elevated in DMD cardiac tissue. (A) Representative fluorescent images of the left ventricle in wild-type and DMD mice (*mdx:utrn*$^{-/-}$*).* The cardiac tissues were stained with Cy5-ghrelin (1-19) and isolectin to show GHSR (purple) and microvessels (green), respectively. Nuclei were visualized with DAPI (blue). Cardiac microvasculature in the DMD heart looks aberrant and have an irregular shape; whereas, in wildtype, microvasculature has the normal circular shape. **(B)** GHSR fluorescence intensity is elevated in DMD mice (n=3, ****$p<0.0001$). Data are represented as mean fluorescence intensity ± SEM. Each bar represents fluorescence intensities from 5 ROIs from each of 5 sections per heart.

3.3 Correlation between LVEF and GHSR

Our previous results have shown a negative correlation between GHSR and Left Ventricular Ejection Fraction (LVEF) in patients who underwent cardiac transplantation.[114] As well, previous work from Dr. Hoffman's group has shown the development of dilated cardiomyopathy in DMD mice at 15 weeks of age.[59] In that study, they performed micro-CT and echocardiography on wild-type and DMD mice to measure LVEF and showed that DMD mice had significantly decreased LVEF compared to WT mice.

To more closely examine the relationship between GHSR and cardiac dysfunction, I performed linear regression analysis on the previously reported LVEF values and Cy5-ghrelin (1-19) fluorescence intensities from the same WT and DMD mice in the present study. There is a strong inverse correlation between LVEF and myocardial GHSR expression (*$p<0.05$, $r = -0.863$). (**Figure 8**).

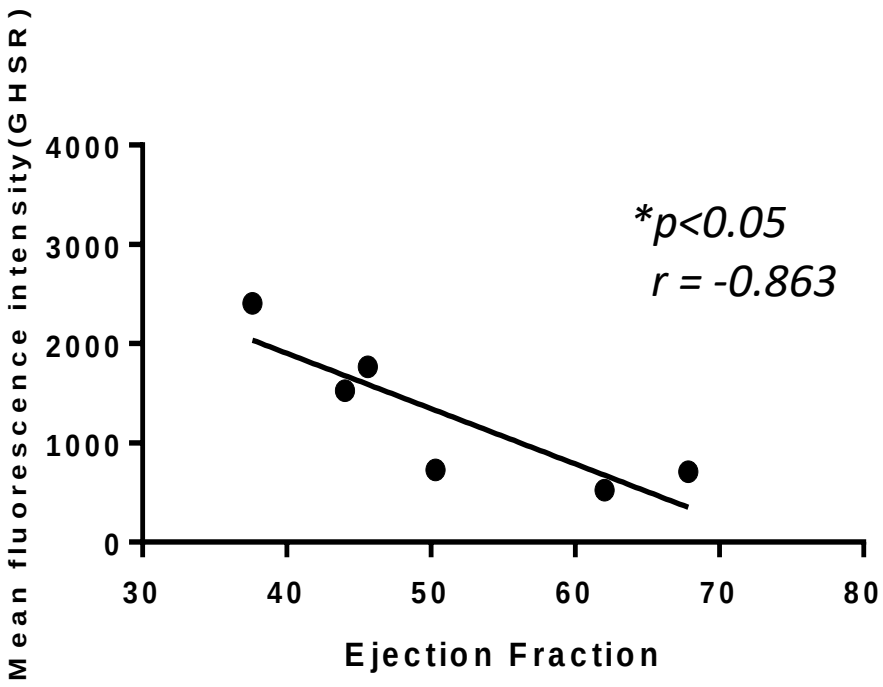

Figure 8. Correlation between ejection fraction (%) and the level of GHSR in cardiac tissues in WT and DMD mice. There is a significant inverse correlation between the ejection fraction and Cy5-ghrelin (1-19) fluorescence intensity in the DMD cardiac tissue. Each data point represents values from one mouse.

3.4 Levels of GHSR correlate with levels of inflammatory markers

To investigate the relationship between GHSR and inflammation, I stained the cardiac tissues with the macrophage marker F4-80 together with Cy5-ghrelin (1-19) and Alexa Fluor 488-isolectin. In WT myocardium, there is low expression of GHSR and no detectable expression of F4-80. AlexaFluor488-isolectin marked the cardiac microvessels in WT myocardium (**Figure 9A**, **top panels**). In contrast, there were markedly higher levels of F4-80 and Cy5-ghrelin (1-19) binding in the left ventricular tissue from DMD mice (**Figure 9A**, **bottom panels**), both of which were significantly different ($p<0.0001$) from WT (**Figure 9B**). Levels of F4-80 and Cy5-ghrelin (1-19) were strongly correlated ($R^2 = 0.97$, $p<0.004$, **Figure 9B**). There were also higher levels of AlexaFluor488-isolectin fluorescence in the DMD myocardium (**Figure 9A**). Upon high-resolution imaging (Figure 10), the fluorescent signals from AlexaFluor488-isolectin and F4-80 overlapped within discrete areas; therefore, AlexaFluor488-isolectin was also labeling macrophages in the DMD myocardium. As well, there was overlap with Cy5-ghrelin (1-19), suggesting that GHSR may be expressed in the cardiac macrophages in DMD myocardium (**Figure 10)**. The identification of macrophages in the cardiac tissue from DMD mice at 15-17 weeks of age indicates chronic inflammation in the DMD myocardium.

Pearson's correlation coefficient of 0.926 between GHSR vs. F4-80 and of 0.784 between isolectin vs. F4-80 indicates colocalization between GHSR and macrophage marker and between the isolectin and the macrophage marker.

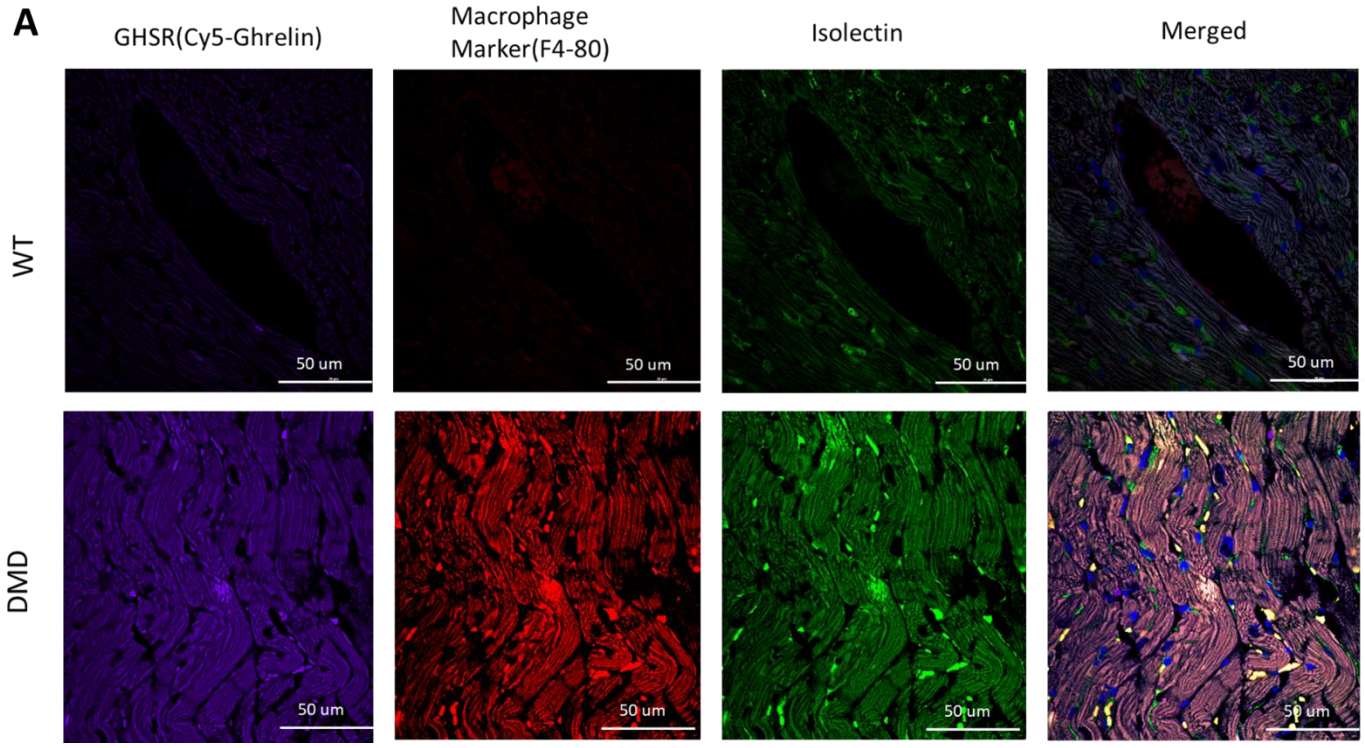
A
GHSR(Cy5-Ghrelin)
Macrophage Marker(F4-80)
Isolectin
Merged
WT
DMD
50 um

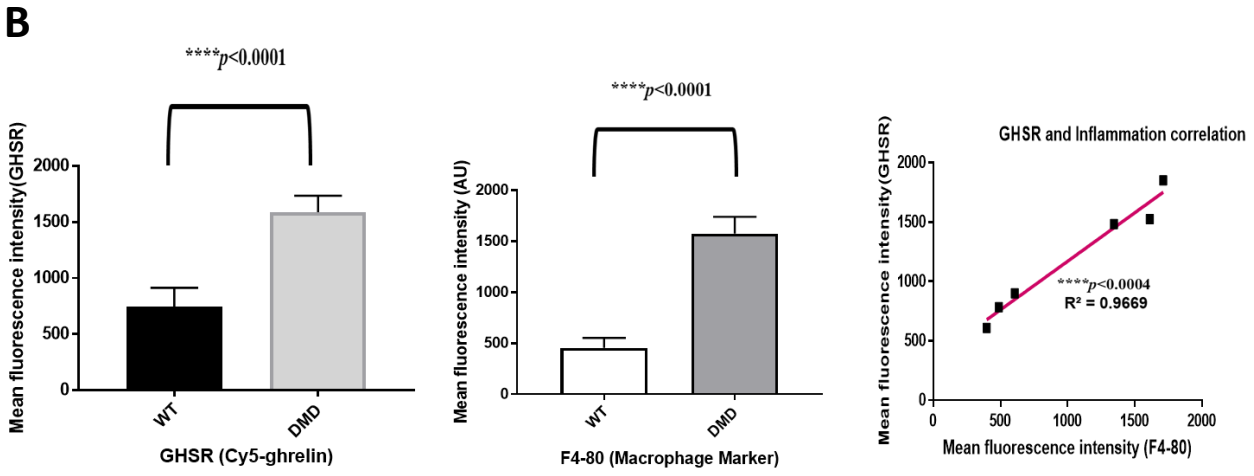
B
****p<0.0001
Mean fluorescence intensity(GHSR)
GHSR (Cy5-ghrelin)
WT
DMD
****p<0.0001
Mean fluorescence intensity (AU)
F4-80 (Macrophage Marker)
GHSR and Inflammation correlation
****p<0.0004
R² = 0.9669
Mean fluorescence intensity (F4-80)

Figure 9. GHSR colocalizes with the macrophage marker F4-80. (A) Representative fluorescent images of the left ventricle in wild-type and DMD (*mdx:utrn*$^{-/-}$*)* mice show Cy5-ghrelin(1-19), F4-80 and isolectin staining to visualize GHSR (purple), macrophages (red) and the vasculature (green), respectively. Nuclei are visualized with DAPI. (B) Quantification of fluorescence intensities for Cy5-ghrelin (1-19) (n=3, ****p<0.0001) and F4-80 (n=3, ****p<0.0001). Data are represented as mean fluorescent intensity ±SEM. Each bar represents fluorescence intensities from 5 ROIs from each of 5 sections per heart. Linear regression analysis indicates a strong correlation between GHSR and F4-80 (****p<0.0004, R^2 =0.9669).

To examine further the relationship between GHSR and inflammation within the myocardium of the left ventricle in DMD mice, I assessed levels of the pro-inflammatory cytokine IL-6, along with Cy5-ghrelin (1-19) and isolectin **(Figure 11A)**. Interestingly, IL-6 expression was also seen in the lumen of the microvessels in the DMD mice, which might be an indicator of monocytes in the lumen, further indicating the extent of inflammation in the left ventricle of DMD mice **(Figure 11A, arrows).** Quantification of fluorescence intensities showed that IL-6 expression levels were significantly greater in DMD myocardium (****p<0.0001) and GHSR was also elevated in DMD (****p<0.0001) (Figure 11B). There was a strong correlation (***p<0.002, R^2 =0.9286) between GHSR and IL-6. (**Figure 11-B).**

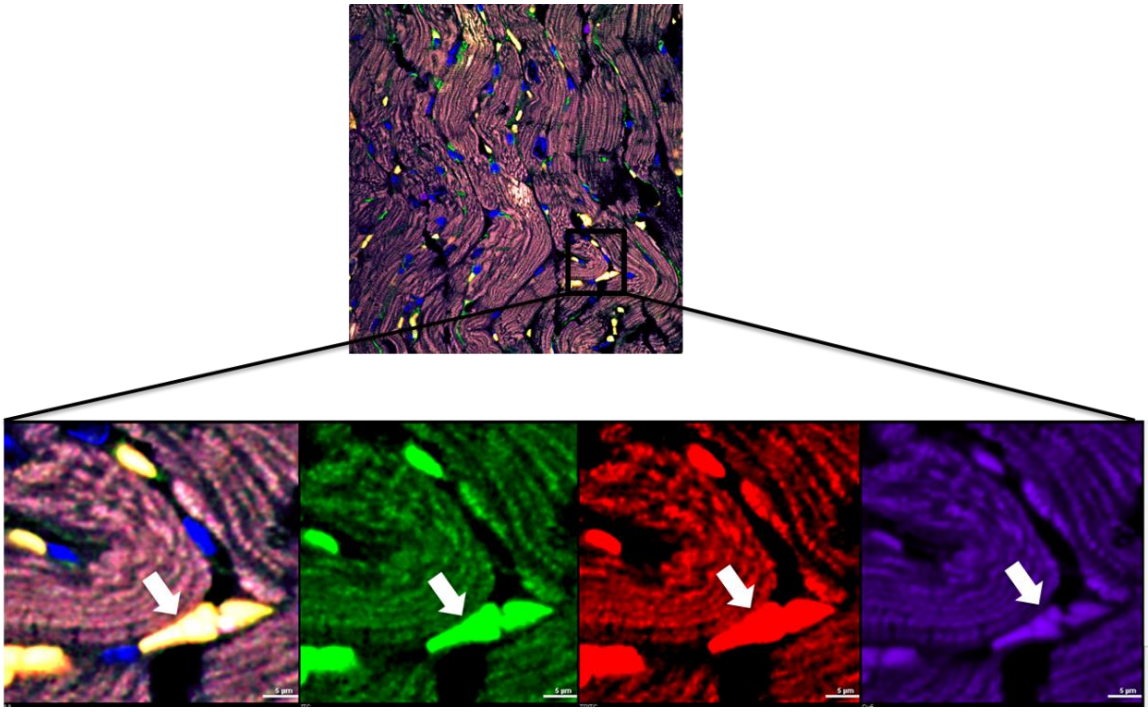

Figure 10. GHSR is expressed in cardiac macrophages. The ROI indicated in the top panel was subject to Nyquist analysis to increase the resolution. Cardiac tissues from DMD mice were stained with Cy5-ghrelin (1-19), F4-80 and isolectin to visualize the GHSR (purple), macrophages (red) and the vasculature (green), respectively. Nuclei were visualized with DAPI. White color indicates the colocalization of the three signals (red, green and purple) which indicates the presence of GHSR in cardiac macrophages (arrows).

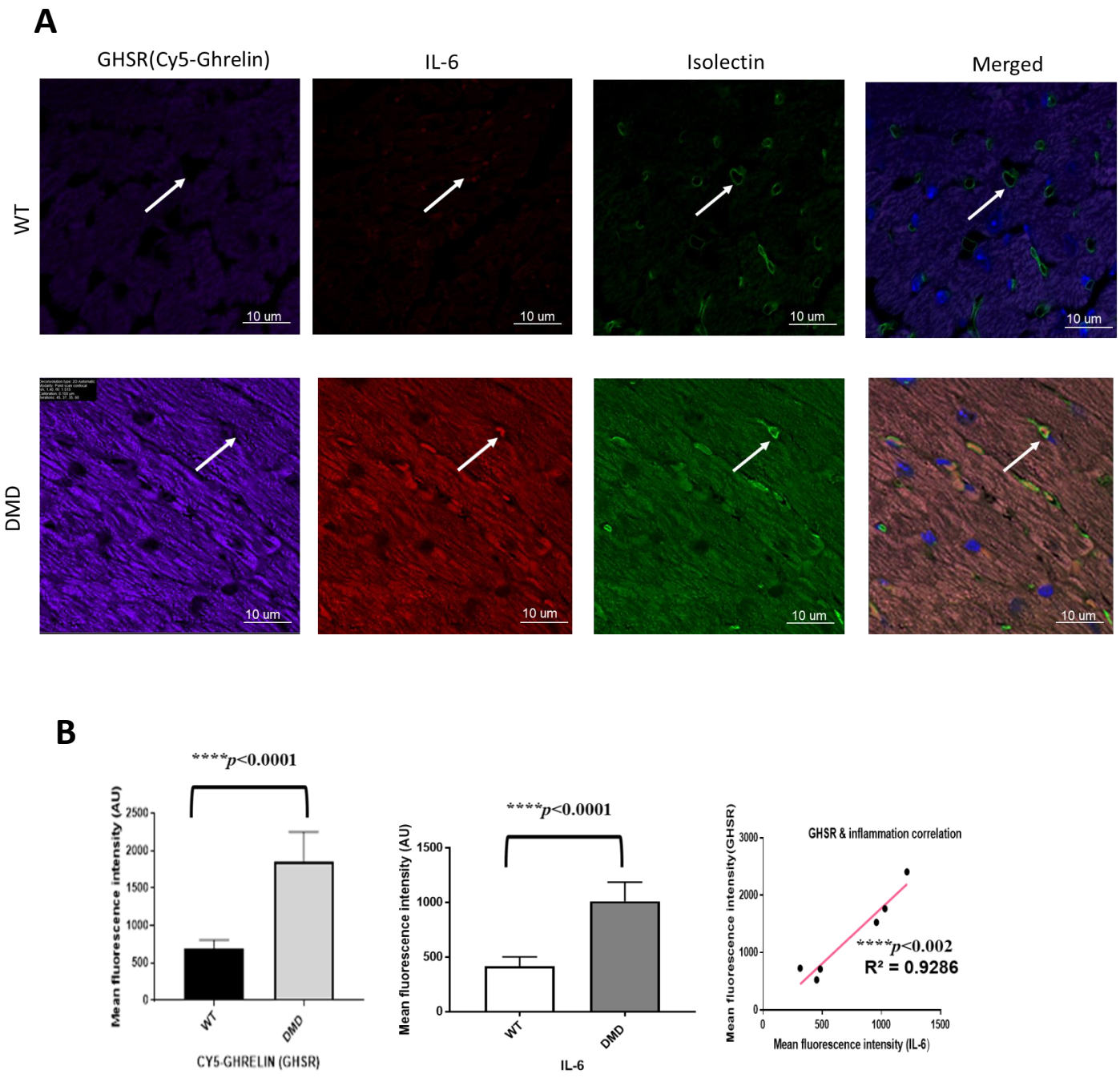

Figure 11. GHSR and the pro-inflammatory cytokine IL-6 are increased in cardiac tissue from DMD mice. (A) Representative confocal fluorescence images of the left ventricular myocardium in WT and DMD (*mdx:utrn*$^{-/-}$) mice. Cardiac tissues were stained with Cy5-ghrelin (1-19), IL-6 and AlexaFluor488-isolectin to visualize GHSR, IL-6 cytokine and the microvessels, respectively. Nuclei were visualized with DAPI. The arrows indicate the cardiac microvessels of WT mice (top row) and IL-6 staining within the microvessels in DMD myocardium (bottom row). **(B)** Quantification of fluorescence

intensities for GHSR (n=3, ****p<0.0001) and IL-6 (n=3, ****p<0.0001). Data are represented as mean fluorescent intensity ±SEM; each bar represents fluorescence intensities from 5 ROIs from each of 5 sections per heart. Linear regression analysis indicates a strong positive correlation for the GHSR vs IL-6 in the cardiac tissues (***p<0.002, R^2 =0.9286).

3.5 GHSR and des-acyl-ghrelin binding in the large cardiac blood vessels.

My results revealed that there is no GHSR in the cardiac microvasculature. Therefore, I asked if the GHSR exists in the large vessels in the heart. Since there is scarce information regarding the binding of des-acyl ghrelin in heart, I co-stained the cardiac tissues with Cy5-ghrelin (1-19) and Cy3-des-acyl- ghrelin (1-19) to determine the binding sites in the large vessels of the vasculature. Interestingly, there was very little to no fluorescence signal in the vasculature (as determined by AlexaFluor488-isolectin staining) of WT mice. In contrast, there was detectable GHSR and des-acyl-ghrelin binding in the DMD cardiac macrovessels. **(Figure 12A).** Quantitative analysis of fluorescence intensities showed that the expression of GHSR (p<0.0001) and binding of Cy3-des-acyl-ghrelin (p<0.001) were both significantly higher within the cardiac microvasculature of DMD mice. **(Figure 12B).**

A

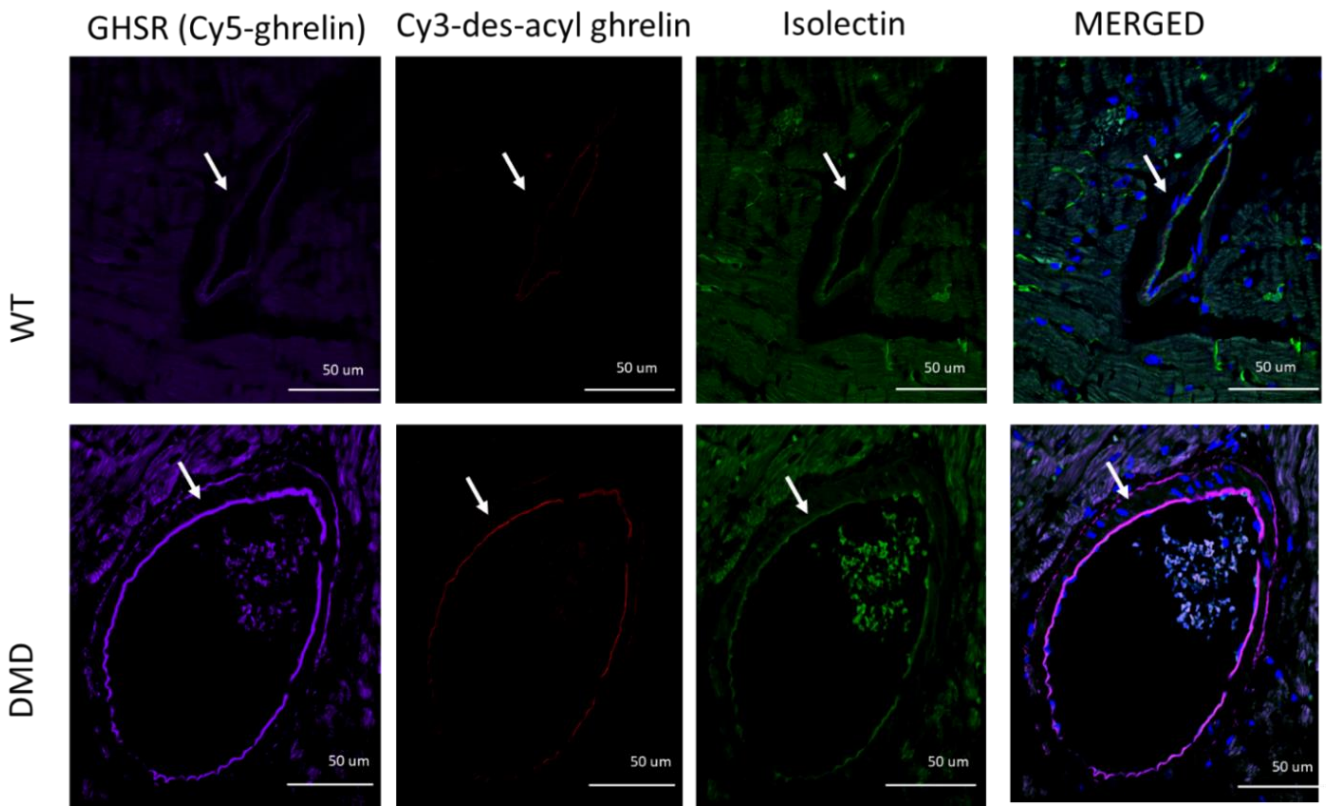

B

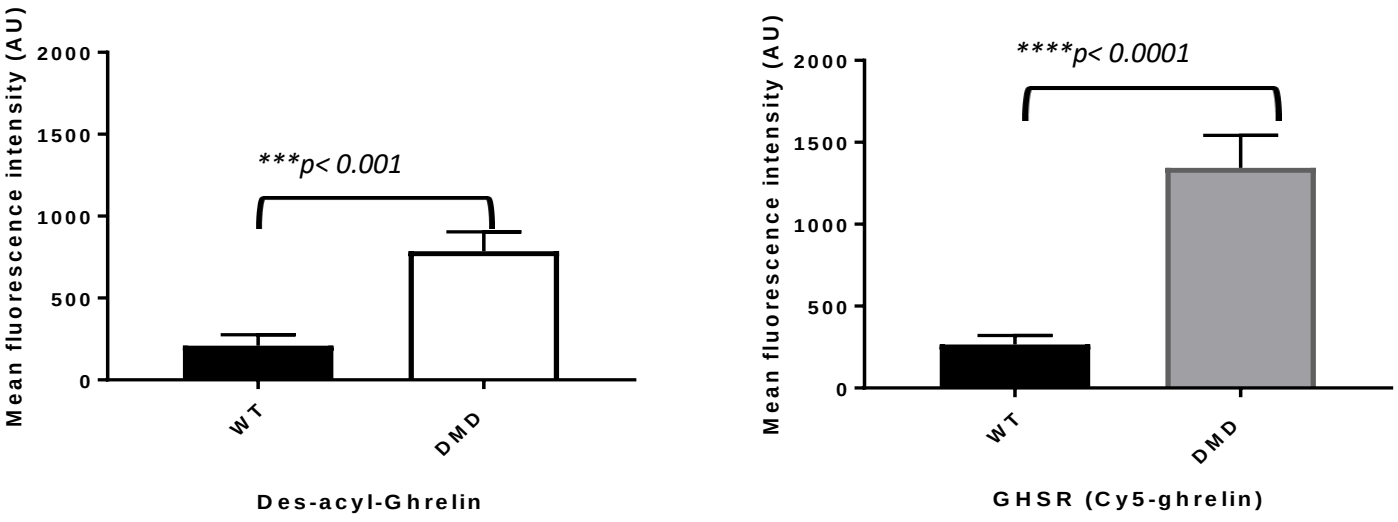

Mean values+S.E.M (n=3)

Figure 12. GHSR and Des-acyl-ghrelin in large vessels in cardiac tissues. (A) Representative fluorescence confocal microscopy images of large vessels in cardiac tissue of wild-type and DMD (*mdx:utrn*$^{-/-}$) mice. The cardiac tissues were stained with Cy5-ghrelin (1-19), Cy3-des-acyl ghrelin (1-19) and AlexaFluor488-isolectin to visualize GHSR, des-acyl-ghrelin binding and the large vessels, respectively. Nuclei were visualized with DAPI. Arrows indicate the large vessel in the cardiac tissues. (B) Quantification of fluorescence intensities for Cy5-ghrelin (1-19) (n=3, ****$p<0.0001$) and Cy3-des-acyl-ghrelin (1-19) (n=3, ***$p<0.001$). Each bar represents fluorescence intensities from 10 ROIs within the vessel structure from each of 5 sections per heart. Data are represented as mean fluorescent intensity ± SEM.

3.6 CD36 in Cardiac tissues

The fatty acid transporter, CD36, is also present on microvascular endothelial cells. There is evidence that CD36 is upregulated in cardiac contractile dysfunction[118]. I assessed the presence of CD36 in myocardial tissue and vasculature in WT and DMD mice. CD36 was present in the microvascular endothelial cells in WT cardiac tissue as assessed by co-localization with AlexaFluor488-isolectin (**Figure 13A**, **top row**). In DMD mice, the pattern of CD36 expression was more widely distributed throughout the tissue in structures that were both isolectin-positive and -negative (**Figure 13A, bottom row**). Quantitative analysis of fluorescence intensities showed that CD36 was present at significantly higher levels in DMD cardiac tissue ($p<0.001$) **(Figure 13B).**

A

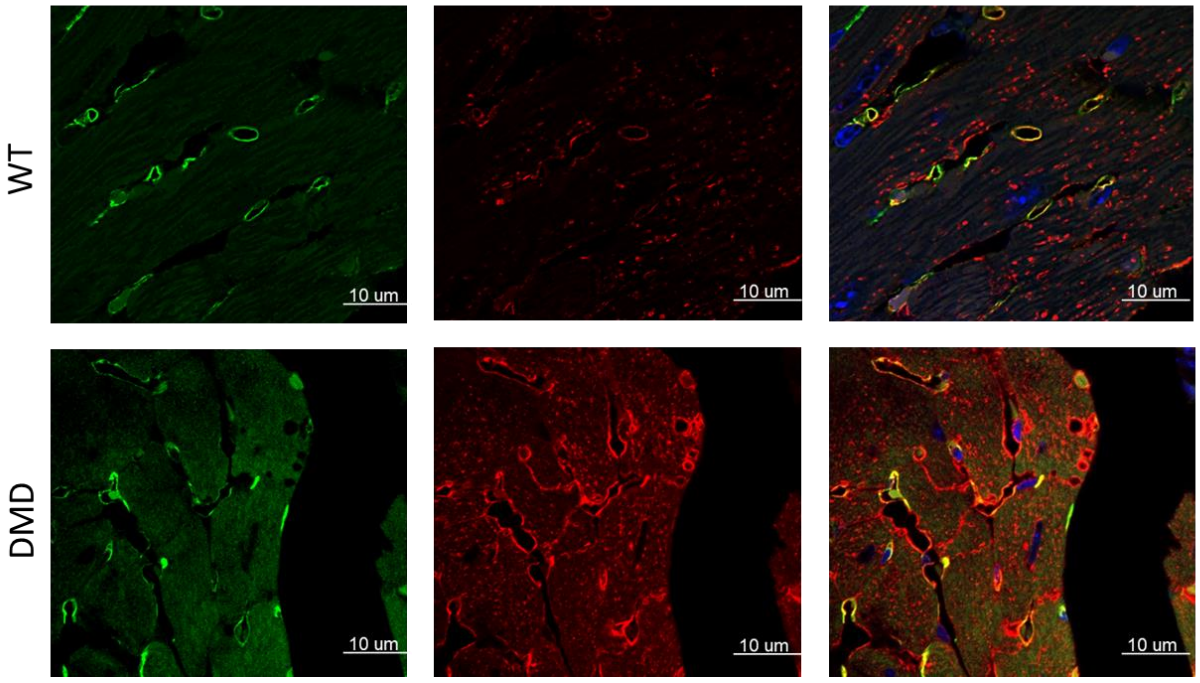

B

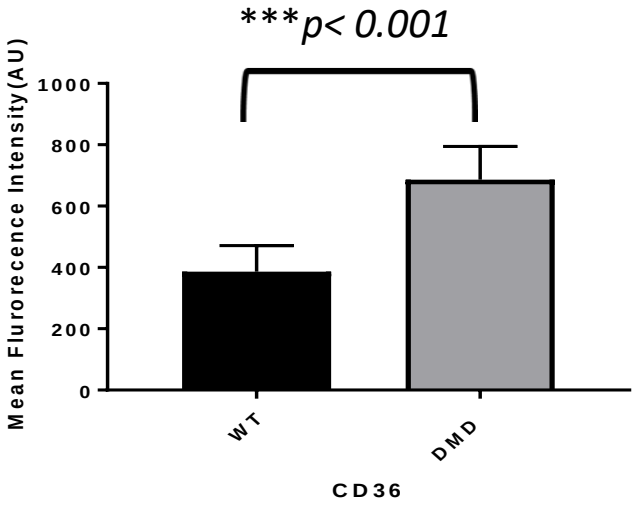

Mean values±S.E.M (n=3)

Figure 13. CD36 levels in the left ventricular myocardium. (A) Representative fluorescent images of left ventricular myocardium in WT and DMD (*mdx:utrn*$^{-/-}$) mice. The cardiac tissues were stained with Cy5-ghrelin (1-19), CD36 and AlexaFluor488-isolectin to visualize GHSR, CD36 and the vasculature, respectively. Nuclei were visualized with DAPI. The CD36 expression is elevated in DMD in microvessels and in other structures which might indicate adipose tissue deposition in the myocardium of DMD mice. (B) Quantification of the fluorescence intensity for CD36 in the WT and DMD cardiac tissues. Each bar represents fluorescence intensities from 5 ROIs from each of 5 sections per heart. Data are represented as mean fluorescent intensity ± SEM (n=3, ***$p<0.001$)

3.7 The effect of the pro-inflammatory cytokine TNFα on GHSR expression in murine cardiac microvascular endothelial cells

To further investigate the connection between GHSR and vascular inflammation, I used cardiac microvascular endothelial cells (MCEC)s that were cultured to confluency and treated with increasing concentrations of TNF-α. Cells were then assessed for GHSR by western blot analysis (**Figure 14A**). Densitometric analysis of the GHSR-immunoreactive bands indicates that a dose of 500 ng/mL of TNFα induces the highest level of GHSR in MCECs (Figure 14B). GHSR levels increased 4.5X upon treatment with 250 ng/ml TNF-α ($p<0.05$), and over 15X upon treatment with 500 ng/ml TNF-α ($p<0.001$), indicating that GHSR is up-regulated in response to a pro-inflammatory stimulus.

A

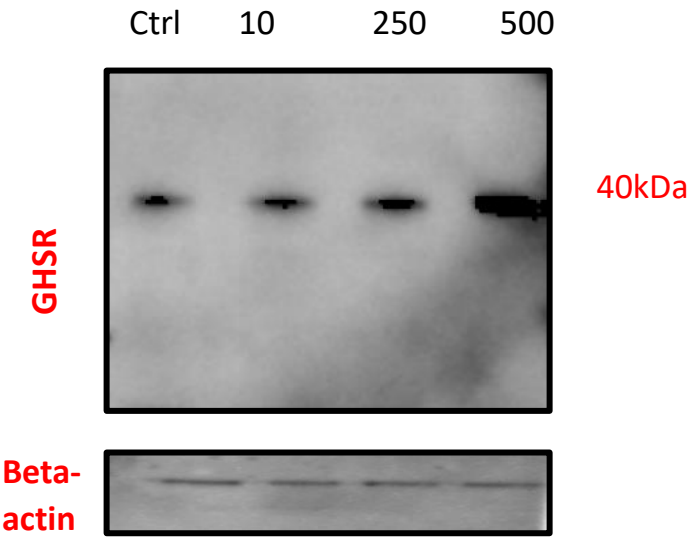

B

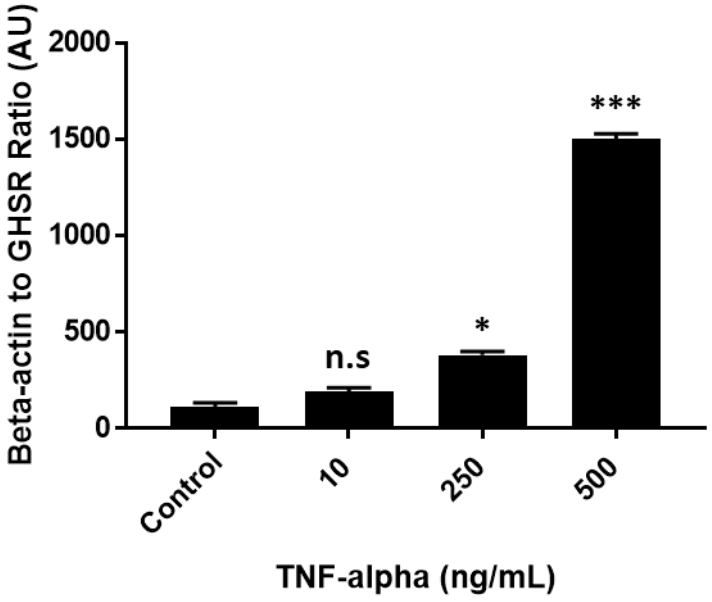

Mean values±S.E.M (n=4)

Figure 14. GHSR increases upon treatment of MCECs with the pro-inflammatory cytokine TNF-α. (A) Cardiac Microvascular Endothelial Cells (MCEC)s were treated with 10, 250 or 500 ng of TNF-α for 16 hours. Cell lysates were collected, and proteins were separated on a 4-12% NUPAGE gel. Membranes were immunoblotted for GHSR and beta-actin. (B) Densitometric analysis of GHSR normalized to β-actin. Data are represented as mean ±SEM and one-way ANOVA was performed on the average of n=4 separate experiments. *$p < 0.05$; ***$p < 0.001$.

To visualize changes in GHSR levels and distribution within MCECs after cytokine stimulation, cells were cultured to confluency, treated with 10, 250 or 500 ng/mL of TNF-α for 16 hours and stained with Cy5-ghrelin (1-19) and DAPI **(Figure 15A).** GHSR expression in MCECs is more cytoplasmic and the level of expression escalated in a dose-dependent manner. 500 ng/mL treatment induced the highest level of GHSR in MCECs ($p < 0.0001$). **(Figure 15B).**

A

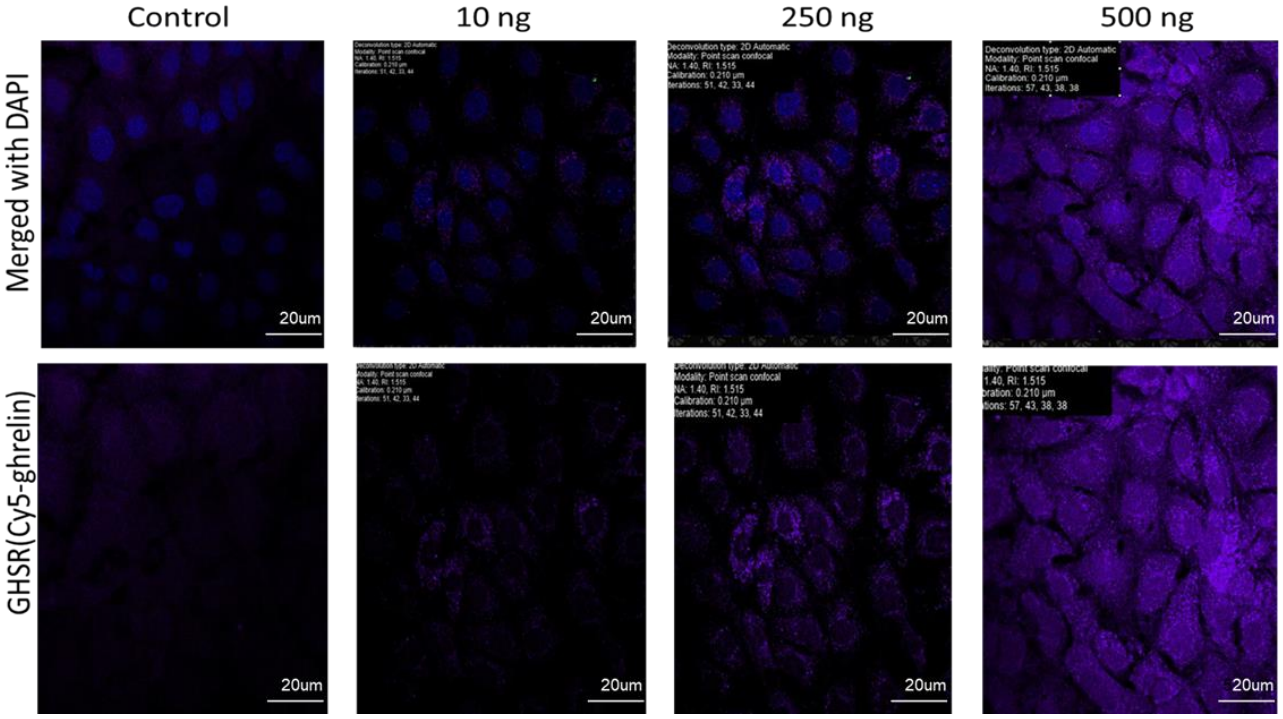

B

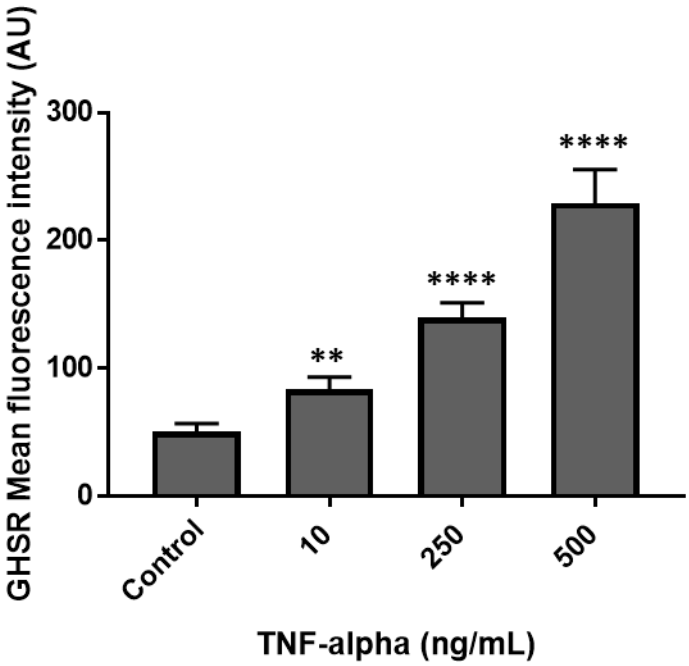

Mean values±S.E.M (n=4)

Figure 15. The level of GHSR increases with cytokine-induced inflammation in cardiac microvascular endothelial cells. (A) Representative fluorescence images from MCECs that were treated with 10, 250 or 500 ng of TNF-α for 16 hours, fixed and stained with Cy5-ghrelin (1-19) and DAPI to denote GHSR and nuclei. (B) Quantification of the fluorescence intensity of Cy5-ghrelin (1-19). Each bar represents fluorescence intensities from 5 ROIs from each of 4 coverslips per treatment. Data represent the mean fluorescent intensity ±SEM and a one-way ANOVA was performed on the average of N=4 separate experiments. **p = 0.0058; ****p < 0.0001; ****p < 0.0001

Upon cytokine stimulation, the level of ICAM increases in the endothelial cells. It is known that TNF-α increases expression of ICAM-1 through the NF-κB pathway and ICAM-1 promotes leukocyte adhesion and increases vascular permeability.[119] [120] My results indicated a dose-dependent increase of GHSR in MCECs treated with TNF-α. My question was whether the increase in GHSR occurred in parallel with an increase in ICAM-1. To answer this question, I treated MCECs with TNF-α and co-stained MCECs for ICAM-1 (green) and with Cy5-ghrelin (1-19) (red). Both GHSR and ICAM-1 appeared as diffuse intracellular signals in MCECs (Figure 16A). Both GHSR and ICAM-1 expression increased in a dose-dependent manner **(Figure 16B)**. However, there was no significant colocalization between GHSR and ICAM-1 in MCECs as assessed by Pearson correlation coefficient. **(Figure 16C).**

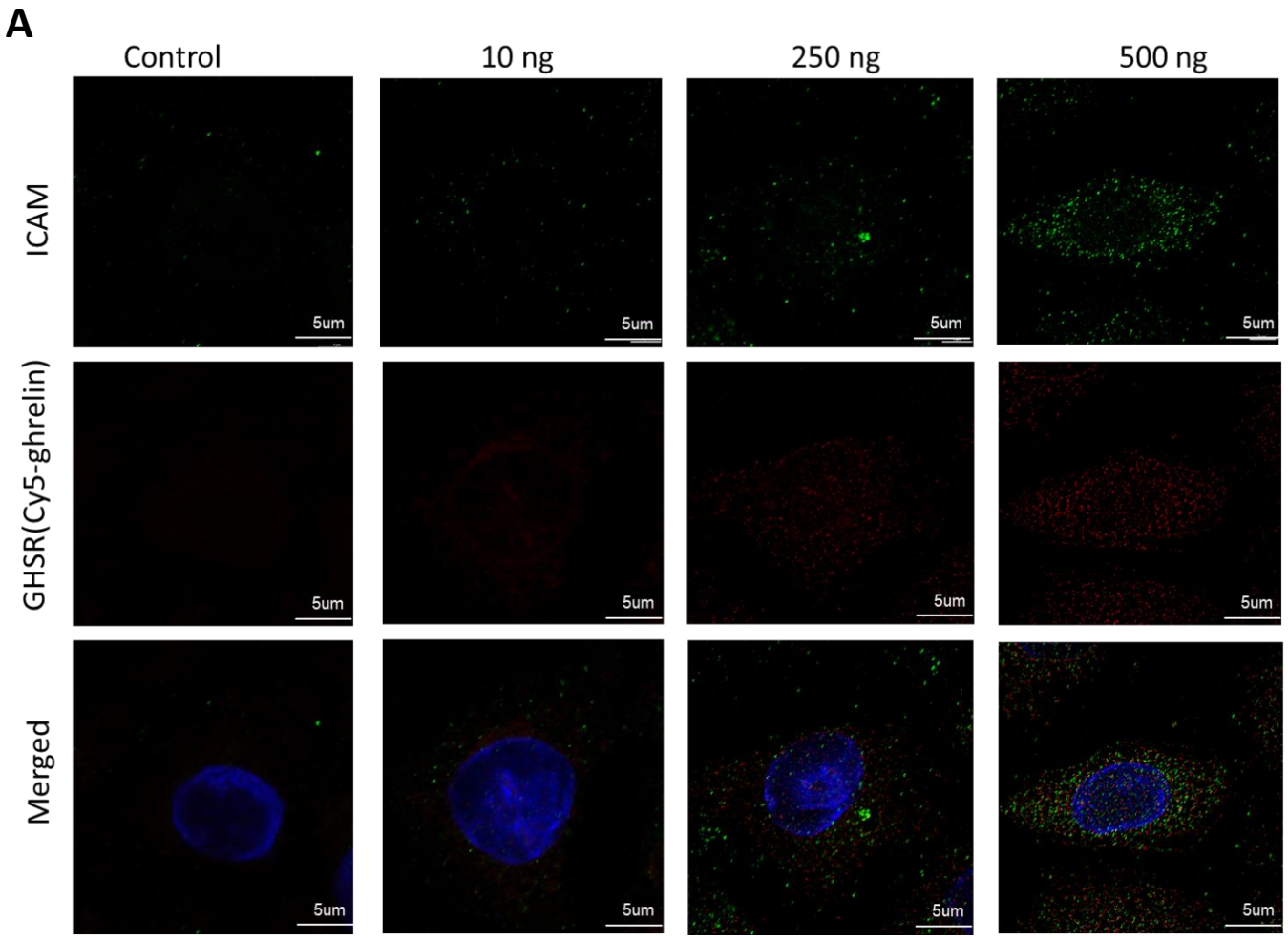
A
Control
10 ng
250 ng
500 ng
ICAM
GHSR(Cy5-ghrelin)
Merged
5um

B

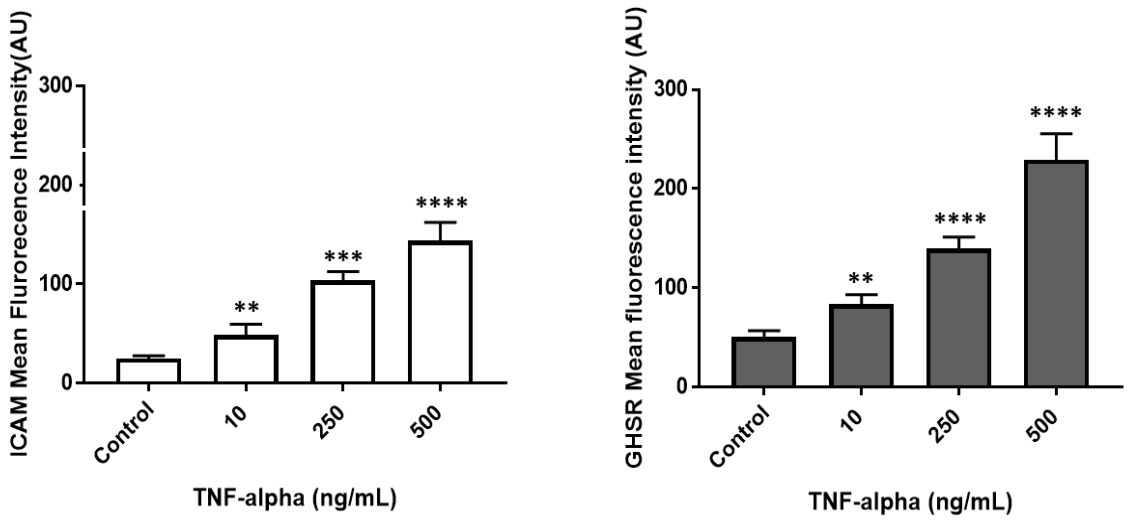

Mean values+S.E.M (n=4)

C

	control	10 ng	250 ng	500 ng
Pearson correlation coefficient(Cy5-ghrelin vs. ICAM)	0.078	0.168	0.246	0.397

Figure 16. GHSR does not colocalize with the ICAM in MCECs treated with TNF-α. (A) Representative fluorescence images from MCECs that were treated with 10, 250 or 500 ng/mL of TNF-α for 16 hours, fixed and permeabilized, and stained with Cy5-ghrelin(1-19), and for ICAM-1 and DAPI. (B) Quantification of the fluorescence intensities of Cy5-ghrelin (1-19) and ICAM-1. Each bar represents fluorescence intensities from 5 ROIs from each of 4 coverslips per treatment. Data represent the mean fluorescent intensity ±SEM and a one-way ANOVA was performed on the average of N=4 separate experiments (ICAM: **p = 0.0013; ****p < 0.002; ****p < 0.0001); (GHSR: **p = 0.0058; ****p < 0.0005; ****p < 0.0001) (C) Pearson's correlation coefficient (PCC) indicate statistic colocalization between the ICAM-1 and Cy5-ghrelin (1-19). Data are represented as average PCC values ±SEM.*p< 0.01, N=4 separate experiments.

Chapter 4

4 Discussion & Future Direction

DMD is an X-linked disease that results from the loss of dystrophin and leads to the development of dilated cardiomyopathy resulting from inflammation, cardiomyocyte death, and fibrosis. Since 90% of DMD patients die due to heart failure, there is an emerging need to understand the cardiac manifestation of DMD. To date, there is no cure for DMD and most therapies for dilated cardiomyopathy have not been successful. For a more beneficial therapy, we need to diagnose dilated cardiomyopathy at an early stage. Identification of tissue-specific biomarkers could open new doors for targeted therapies. In the work described in this thesis, I sought to characterize the cardiac pathology in a mouse model of DMD, *mdx:utrn*$^{-/-}$, and to investigate whether GHSR could be a biomarker for DMD dilated cardiomyopathy.

Briefly, the main objectives were: 1. To characterize GHSR and inflammatory markers in cardiac tissues in a mouse model of DMD; and 2. To characterize GHSR in vascular endothelial cells and determine its correlation with the level of inflammation.

4.1 Characterization of cardiac tissue pathology in the *mdx:utrn*$^{-/-}$ mouse

This is the first study that has evaluated the extent of cardiac degeneration in *mdx:utrn*$^{-/-}$ mice via histological techniques. Studies from our lab had previously measured functional changes during the development of dilated cardiomyopathy *in vivo* in the *mdx:utrn*$^{-/-}$ mouse model at 15-17 weeks of age with micro-CT and echocardiography. [59] The

histopathology of the skeletal muscle, but not the cardiac muscle, has been previously characterized by other research groups, including our group.[121] [122] [123] [124] In this study, I focused more on examining the left ventricle of DMD mice since in DCM, the left ventricle is mainly affected and also cardiac MRI has confirmed the particular involvement of the left ventricle in DMD patients. [21] [125]

The gold standard histopathology staining, H&E, for *mdx:utrn*$^{-/-}$ mice detailed the extent of chronic inflammation in cardiac tissues at 15-17 weeks of age. It showed the existence of lymphocyte aggregates in the lateral wall and apex of the left ventricle that is a hallmark of chronic inflammation. Pyknosis is a feature of myocardial necrosis which is sparse and more focal in *mdx:utrn*$^{-/-}$ mice, and it triggers macrophage migration to the site of tissue damage and cell death.[76] [126]

Cardiomyocyte vacuolation also presents in these mice which is another feature of myofiber necrosis and cardiomyopathy. Electron microscopy has shown that the vacuolization occurs due to damage in mitochondria or smooth endoplasmic reticulum (SER) which leads to sarcolemmal swelling and necrosis. The mechanism of the mitochondrial or SER damage is poorly understood but it may occur due to impairments in the ATP-dependent ion pump in the mitochondrial and SER membranes.[127] [128] Cardiomyocyte vacuolization may also be the result of impaired blood flow associated with endothelial dysfunction and ischemia.[129]

Fat deposition or lipomatosis in the DMD myocardium is a hallmark of chronic cardiomyopathy. Adipose tissue infiltration interferes with the intercalated disks that allow for synchronization of cardiomyocyte beating leading to arrhythmias and causing sudden

death. However, the mechanism by which adipose tissue forms and get stored in cardiomyopathy remains unknown. [45] [130]

Fibrosis in the myocardium was detected in the left ventricle by Masson's Trichrome staining. Fibroblasts form a fibrocollagenous scar tissue replacing cardiomyocytes, thereby impairing myocardial contraction. This myocardial fibrosis in the *mdx:utrn*$^{-/-}$ mice was very diffuse, and there was more collagen deposition in the apex compared to the lateral wall of the left ventricle. This fibrotic pattern is very similar to what is seen in DMD patients and it is unique to dystrophinopathies. [30] [131]

4.2 GHSR is elevated in myocardium of the *mdx:utrn*$^{-/-}$ mouse

Having characterized the morphological changes of dilated cardiomyopathy in the *mdx:utrn*$^{-/-}$mouse model, I investigated whether myocardial GHSR levels are altered in our model as assessed by the binding of our imaging probe, Cy5-ghrelin(1-19). With using this fluorescent peptide analog of ghrelin, our lab has previously shown that GHSR levels are altered before and after cardiac transplantation in humans, [114] and also in diabetic cardiomyopathy in mice .[113] My results showed an elevation in GHSR in the myocardium of the *mdx:utrn*$^{-/-}$ mice at end-stage cardiomyopathy, which is in agreement with the elevated levels of GHSR that our lab has reported in end-stage human heart failure.[114] However, my results are in contrast with the mouse diabetic cardiomyopathy studies, where the level of GHSR is down-regulated using both fluorescence microscopy with Cy5-ghrelin(1-19) and Western blot analysis.[113] The reason for this discrepancy between the mice with diabetic cardiomyopathy and the *mdx:utrn*$^{-/-}$ mice could be possibly explained by the fact that they were in different stages of cardiac disease. Diabetic cardiomyopathy

mouse model showed very mild changes in heart function and no sign of inflammation or fibrosis. In contrast, the *mdx:utrn*$^{-/-}$ mice had late-stage cardiomyopathy, with a highly fibrotic and inflammatory pathology. Therefore, I suggest that GHSR is elevated in late-stage cardiomyopathy, and down-regulated in early stage cardiomyopathy in mice.

4.3 Correlation between left ventricular function, cardiac pathology and GHSR

The functional features of dilated cardiomyopathy are an increase in left ventricular volume and decrease in EF.[62] Previously, echocardiography and micro-CT had been performed on my experimental mice to show that LVEF was decreased.[59] This decline in LVEF in DMD mice may also result in the severe pathology of the LV apex detailed in my study. It has been proposed that the apex of the heart may be the most susceptible region of the heart for thrombus formation due to lowered blood flow, which occurs in dilated cardiomyopathy. To this end, there are reports on apical thrombus in DCM- affected subjects which support this probable mechanism. [132] [133] [134]

My data showed a negative correlation between GHSR levels and LVEF. These results support our recent findings, which also demonstrated a negative correlation between the LVEF and GHSR levels in patients who underwent cardiac transplantation.[114] I speculate that the elevated levels of GHSR in end-stage cardiomyopathy may be due to abnormal signaling of pro-survival pathways in response to cardiomyocyte damage, necrosis and apoptosis. These results suggest that GHSR may be an effective biomarker of LV function in DMD cardiomyopathy.

4.4 Chronic inflammation correlates with GHSR in DMD left ventricle

This study is the first of its kind to correlate levels of GHSR with cardiac inflammation, as detected by macrophage infiltration and tissue cytokines. A notable feature of chronic inflammation is the existence of lymphocytes and macrophages. Since H&E staining cannot differentiate between lymphocytes and macrophages, we used fluorescence immunostaining using F4-80 as a macrophage marker to detect the existence of macrophages in the DMD myocardium. In chronic inflammation, both M1 (pro-inflammatory) and M2 (regeneration) macrophages are present.[135] However, F4-80 cannot differentiate between M1 and M2 macrophages. To evaluate the macrophage phenotypic distribution, we need to use CD11c for M1 and CD206 as a marker of M2.[136] Macrophages implements a range of important immunoregulatory and inflammatory functions by secreting chemokines and cytokines and also by degrading the extracellular matrix that surrounds cardiomyocytes. Damaged cardiomyocytes activate pro-inflammatory signaling pathways through NF-κB which upregulates the production of pro-inflammatory cytokines such as TNF-α, IL-1 and IL-6. As well, the Toll-like receptor (TLR) family also plays an important role in tissue inflammation and cell death. Specifically, TLR4 was shown to be involved in DMD pathogenesis, as TLR4 genetic ablation in *mdx* mice resulted in dramatic blunting of macrophages, reduced fibrogenesis and increased capacity of skeletal muscle regeneration. [137]. TLR4 could be one of the key mediators in dilated cardiomyopathy since it initiates cytokine activation in damaged cardiomyocytes.[138] Therefore, the dilated cardiomyopathy of DMD is highly inflammatory, and this process is mediated by both macrophages and cardiomyocytes.

My study has shown for the first time that GHSR is expressed in DMD murine macrophages in the myocardium. The expression of GHSR in macrophages may indicate a new role for ghrelin/GHSR in inflammation. A study showed that GHSR ablation in aged mice reduced the macrophage infiltrates and also promoted the macrophage phenotypical shift towards M2 (anti-inflammatory phase).[139] As well, GHSR is present and elevated in alveolar macrophages during sepsis-induced acute respiratory distress syndrome in rats, [140] and ghrelin administration inhibited GHSR signaling through the Wnt/β-catenin pathway, reducing apoptosis and inflammation.

My studies show an increase in the expression of the cytokine IL-6 in the cardiac tissue of DMD mice. These results are in agreement with the literature, which shows high levels of IL-6 in the serum and inflammatory infiltrates of DMD patients. There is evidence that IL-6 is elevated in the diaphragm muscle of *mdx* mice.[141] [142] In the heart, IL-6 has dual roles in both cardioprotection and cardiac failure. In acute inflammation, IL-6 participates in neurogenesis and wound healing and maintains cardiac integrity. In contrast, in chronic inflammation, IL-6 activates constant signaling through the NF-kB pathway which leads to fibrosis.[143] My results suggest that the elevated levels of IL-6 are due to chronic inflammation that will eventually lead to heart failure. There is a strong correlation between IL-6 and GHSR in DMD which indicate GHSR involvement in inflammation. This data may suggest that in inflammatory condition, GHSR is elevated to prevent apoptosis through PI3K and ERK1/2 pathway and also promote cell proliferation through PI3K and AKT pathway.

4.5 GHSR and des-acyl-ghrelin binding sites in the cardiac vasculature

My studies showed that there is no GHSR expression in cardiac microvasculature in both WT and DMD mice. I also showed that the arrangement of the microvasculature is aberrant in the DMD myocardium, which may cause left ventricle microinfarct which leads to necrosis. [77] [144] However, the interpretation of these findings are limited, as AlexaFluor488-isolectin marked the microvasculature in WT mice, but was not specific to the vasculature in DMD mice, and also stained the murine macrophages.

My results showed that there is binding of both Cy5-ghrelin (1-19) and Cy3-des-acyl ghrelin (1-19) in the cardiac macrovasculature, but not the microvasculature, in the DMD mouse. No binding of either probe was evident in the large vessels of WT mice. In contrast to Cy5-ghrelin (1-19), the binding of Cy3-des-acyl ghrelin (1-19) was observed only in the large blood vessels, and not in cardiomyocytes. Its colocalization with isolectin in the vessel wall, but not in cells within the lumen of the vessel, suggests that des-acyl ghrelin binding sites are on endothelial cells.[112] The elevated ghrelin and des-acyl ghrelin binding in the DMD mouse might be an indicator of inflammation within large cardiac vessels.

This is the first demonstration of both ghrelin and des-acyl-ghrelin binding in cardiac vasculature. I was able to detect binding sites for both ghrelin and des-acyl ghrelin in the same tissue due to our fluorescent ghrelin analogs which are very specific; Cy5-ghrelin (1-19) binds specifically to GHSR in the mouse myocardium whereas Cy3-des-acyl-ghrelin (1-19) does not.[112] Interestingly, it has been shown that des-acyl ghrelin inhibits cell death in endothelial cells through ERK1/2 signaling, but the receptor remains unknown.[97]

4.6 CD36 in Cardiac tissues

CD36 is a fatty acid transporter. Normally, CD36 marks the microvascular endothelial cells in cardiac tissue, and under conditions of inflammation, CD36 is also expressed in cardiomyocytes, which could be evidence of cardiac dysfunction.[145] In the DMD cardiac tissue, CD36 no longer appeared to be restricted to the microvasculature structure, which had lost the cylindrical structure and appeared aberrant.[144] Our histopathology showed adipose tissue infiltration in DMD cardiac tissue; coupled with the observation of CD36 immunoreactivity in isolectin-negative structures. Therefore, I suggest that the increase in CD36 may be due to this adipose tissue infiltration. It has been shown that CD36 increases in age-induced cardiomyopathy in mice as it is a major regulator of cardiomyocyte fatty acid uptake in cardiomyocytes.[146] This finding suggests that the elevation in CD36 may promote myocardial lipotoxicity in *mdx:utrn*$^{-/-}$ mice.

4.7 The effect of the pro-inflammatory TNF-α on GHSR expression in murine cardiac microvascular endothelial cells

For preliminary mechanistic studies, I further explored the relationship between GHSR and inflammation in murine cardiac microvascular endothelial cells (MCECs). My experiments revealed that there is an expression of GHSR in MCECs and it is elevated upon exposure to the pro-inflammatory cytokine TNF-α in a dose-dependent manner. These results are consistent with my animal studies that showed a positive correlation between GHSR and the pro-inflammatory cytokine IL-6 and the macrophage marker F4-80. However, there is a discrepancy, in that I found GHSR to be present in the large vessels of cardiac tissues under conditions of chronic inflammation, but not in the microvasculature. This apparent

discrepancy may be due to the fact that MCECs is an immortalized neonatal cell line, and the mouse tissues I used in this study, were from adult mice. Furthermore, to generate the MCECs, cardiac microvascular endothelial cells had been transfected by lentiviral vectors which carry the SV40 large T antigen and human telomerase. This cell line displays normal characteristics of endothelial cells but through genetic modification, some cellular functions may be altered and it's a limitation for the cell studies. Therefore, GHSR expression in the neonatal microvascular endothelial cell line, but not in adult mouse cardiac microvascular endothelial cells, may indicate a role for ghrelin/GHSR in the maturation of these cells from the neonatal to adult stage.

In endothelial cells, TNF-α increases expression of ICAM-1 through the NF-kB pathway and ICAM-1 promotes leukocyte adhesion and increases vascular permeability.[119] [120] ICAM-1 expression was also increased in a dose-dependent manner but it didn't colocalize strongly with GHSR in our model. The significance of these findings requires further investigations.

4.8 Future Directions

We demonstrated that GHSR could be a biomarker for inflammation in dilated cardiomyopathy in *mdx:utrn*$^{-/-}$ mice. To show the patterns in GHSR levels during the development of DCM in this mouse model, we need to conduct the experiments outlined in this thesis (correlation between inflammatory markers and GHSR) at earlier time points such as 4-5 and 8-10 weeks of age. 4-5 weeks of age is a very early stage of DMD with no

symptoms of cardiomyopathy; at 8-10 weeks of age, dilative cardiomyopathy is starting to develop in *mdx:utrn*$^{-/-}$ mice.[59]

Future studies should introduce intravital microscopy along with the confocal microscopy and measure the blood flow in DMD vasculature and compare it with WT. This study will provide dynamic data on blood flow which could give more insight about DMD vasculature and how ghrelin-derived therapeutics could affect or correct the vascular structure.[147]

Multiphoton laser scanning microscopy also could be used to study the DMD heart in depth. This microscope enables us to do the 3D histology and in vivo imaging of the heart with high-resolution and high-speed. With this microscope, we could visualize the beating heart in vivo with subcellular resolution and we could study the migration of leukocytes into the inflamed vasculature and cardiac tissue.[148]

For mechanistic studies to establish the relation of inflammation and GHSR in endothelial cells, we need to silence GHSR through siRNA and determine how TNF-α induced inflammation affects inflammatory signaling pathways (E-selectin, AKT, PI3K and VE-cadherin) in endothelial cells by western blot, IF and ELISA.

To determine whether ghrelin has an anti-inflammatory effect on the endothelial cell, we could treat the MCECs with hexarelin (a GHSR agonist which is more stable than ghrelin) at different time points (30 min,70 min,6,24,48,72 hours) and determine the level of inflammation by western blot, IF and ELISA.

Several studies demonstrated that ghrelin administration may improve skeletal muscle mass and function in mdx mice . [149] [150] [151] In future studies, we could administer ghrelin and des-acyl ghrelin to *mdx:utrn*$^{-/-}$ mice and measure the pro-inflammatory cytokines in

plasma and also determine the level of GHSR and inflammatory markers in cardiac tissue and vasculature. This will elucidate whether ghrelin could be used as a therapeutic for DMD cardiomyopathy.

4.9 Concluding remarks

This study provides insight into the imaging GHSR *in situ* in DMD dilated cardiomyopathy. With the specific probe, Cy5-ghrelin (1-19), I showed a strong positive correlation between GHSR and inflammation markers which may suggest that GHSR could be a possible biomarker for chronic inflammation in dilated cardiomyopathy. The negative correlation between GHSR and LVEF proposed the GHSR as a heart function biomarker.

Despite the advancements in imaging and biomarkers research for cardiomyopathy, distinguishing early pathogenesis and understanding disease mechanisms remain unsolved. Innovations in early recognition of cardiomyopathy can improve the survival and quality of life for patients and reduce the disease progression and hospital admission rate. These advancements also can open new doors for targeted therapies. Imaging GHSR in *mdx:utrn*$^{-/-}$ mice represent a step towards the detection of early biomarkers for inflammation and dilated cardiomyopathy.

References:

1. Yusuf, S., Reddy, S., Ounpuu, S. & Anand, S. Clinical Cardiology : New Frontiers Global Burden of Cardiovascular Diseases. *Circulation* **104,** 2746–2753 (2001).
2. MOGE(S) a standardized classificafication of cardiomyopathy? *Nat. Rev. Cardiol.* **11,** 134–135 (2014).
3. Tran, D. T. *et al.* The current and future financial burden of hospital admissions for heart failure in Canada: a cost analysis. *C. Open* **4,** E365–E370 (2016).
4. Corrado, D. *et al.* Contemporary Definitions and Classification of the Cardiomyopathies. *Circulation* **113,** 1807–1816 (2006).
5. Westphal, J. G. *et al.* The MOGE(S) classification for cardiomyopathies: current status and future outlook. *Heart Fail. Rev.* **22,** 743–752 (2017).
6. Briceno, N., Schuster, A., Lumley, M. & Perera, D. Ischaemic cardiomyopathy: pathophysiology, assessment and the role of revascularisation. *Heart* **102,** 397–406 (2016).
7. McKenna, W. J., Maron, B. J. & Thiene, G. Classification, epidemiology, and global burden of cardiomyopathies. *Circ. Res.* **121,** 722–730 (2017).
8. Keren, A. *et al.* Classification of the cardiomyopathies: a position statement from the european society of cardiology working group on myocardial and pericardial diseases. *Eur. Heart J.* **29,** 270–276 (2007).
9. Christiaans, I. & Elliott, P. M. Hypertrophic cardiomyopathy. *Clin. Cardiogenetics Second Ed.* **381,** 61–74 (2016).
10. Colan, S. D. Classification of the cardiomyopathies ☆. *Prog. Pediatr. Cardiol.* **23,** 5–15 (2007).
11. López-Cuenca, D., Muñoz-Esparza, C., Navarro Peñalver, M., García Alberola, A. & Gimeno Blanes, J. R. Hypertrophic or hypertensive cardiomyopathy? *Int. J. Cardiol.* **203,** 891–892 (2016).
12. Kirkels, J. H. & de Jonge, N. Restrictive cardiomyopathy. *Circ. Res.* **121,** 819–837 (2017).
13. Kucera, F. & Fenton, M. Update on restrictive cardiomyopathy. *Paediatrics and Child Health (United Kingdom)* **27,** 567–571 (2017).
14. Zangwill, Steven.Hamilton, R. Restrictive cardiomyopathy. **32,** 41–43 (2009).
15. Indik, J. H. & Marcus, F. I. Arrhythmogenic Right Ventricular Cardiomyopathy. *Hear. Fail. Child Young Adult From Bench to Bedside* **373,** 291–296 (2017).
16. Basso, C., Corrado, D., Marcus, F. I., Nava, A. & Thiene, G. Arrhythmogenic right ventricular cardiomyopathy. *Lancet* **373,** 1289–1300 (2009).
17. Maron, B. J. *et al.* Contemporary Definitions and Classification of the Cardiomyopathies. *Circulation* **113,** 1807–1816 (2006).
18. Sisakian, H. Cardiomyopathies: Evolution of pathogenesis concepts and potential for new therapies. *World J. Cardiol.* **6,** 478–494 (2014).
19. Taylor, M. R. G., Carniel, E. & Mestroni, L. Cardiomyopathy, familial dilated. *Orphanet J. Rare Dis.* **8,** 1–8 (2006).
20. Codd, M. B., Sugrue, D. D., Gersh, B. J. & Iii, L. J. M. Epidemiology of Idiopathic

Dilated and Hypertrophic Cardiomyopathy. *Circulation* **80,** 564–572 (1989).
21. Patel, M. D. *et al.* Pediatric and adult dilated cardiomyopathy represent distinct pathological entities. *JCI Insight* **2,** 1–16 (2017).
22. Cowie, M. R., Cook, S. A., Prasad, S. K., Japp, A. G. & Gulati, A. The Diagnosis and Evaluation of Dilated Cardiomyopathy. *J. Am. Coll. Cardiol.* **67,** 2996–3010 (2016).
23. Colan, S. D. Classification of the cardiomyopathies. *Prog. Pediatr. Cardiol.* **23,** 5–15 (2007).
24. Elliott, P. *et al.* Classification of the cardiomyopathies : a position statement from the european society of cardiology working group on myocardial and pericardial diseases. *Eur. Heart J.* **29,** 270–276 (2008).
25. Robson, L. G. Experimental Models of Duchenne Muscular Dystrophy: Relationship with Cardiovascular Disease. *Open Cardiovasc. Med. J.* **4,** 265–277 (2010).
26. Mavrogeni, S. *et al.* Cardiac profile of asymptomatic children with Becker and Duchenne muscular dystrophy under treatment with steroids and with/without perindopril. *BMC Cardiovasc. Disord.* **17,** 1–6 (2017).
27. Johnstone, V. P. A., Viola, H. M. & Hool, L. C. Dystrophic Cardiomyopathy-Potential Role of Calcium in Pathogenesis, Treatment and Novel Therapies. *Genes (Basel).* **8,** 108 (2017).
28. Mcnally, E. M. & Macleod, H. Therapy Insight : cardiovascular complications associated with muscular dystrophies. *Nat. Publ. Gr.* **2,** 301–308 (2005).
29. Mercuri, E. & Muntoni, F. Muscular dystrophies. *Lancet* **381,** 845–860 (2013).
30. Kamdar, F. & Garry, D. J. Dystrophin-Deficient Cardiomyopathy. *J. Am. Coll. Cardiol.* **67,** 2533–2546 (2016).
31. Mercola, M., Ruiz-lozano, P. & Schneider, M. D. Cardiac muscle regeneration : lessons from development. *Genes Dev.* **25,** 299–309 (2011).
32. Woolf, P. J. *et al.* Alterations in dihydropyridine receptors in dystrophin-deficient cardiac muscle. *Am. J. Physiol. Circ. Physiol.* **290,** 2439–2445 (2006).
33. Fayssoil, A., Nardi, O., Orlikowski, D. & Annane, D. Cardiomyopathy in Duchenne muscular dystrophy: pathogenesis and therapeutics. *Heart Fail. Rev.* **15,** 103–107 (2010).
34. Whitehead, N. P., Yeung, E. W., Froehner, S. C. & Allen, D. G. Skeletal Muscle NADPH Oxidase Is Increased and Triggers Stretch-Induced Damage in the mdx Mouse. *PLoS One* **5,** 15354 (2010).
35. Ennen, J. P., Verma, M. & Asakura, A. Vascular-targeted therapies for Duchenne muscular dystrophy. *Skelet. Muscle* **3,** 1–12 (2013).
36. Bushby, K. *et al.* Diagnosis and management of Duchenne muscular dystrophy , part 1 : diagnosis , and pharmacological and psychosocial management. *Lancet Neurol.* **9,** 77–93 (2010).
37. D'Amario, D. *et al.* A current approach to heart failure in Duchenne muscular dystrophy. *Heart* **103,** 1770–1779 (2017).
38. Abdel-Salam, E., Abdel-Meguid, I. & Korraa, S. S. Markers of degeneration and regeneration in Duchenne muscular dystrophy. *Acta Myol.* **28,** 94–100 (2009).
39. Saito, K. *et al.* A sensitive assay of tumor necrosis factor α in sera from Duchenne muscular dystrophy patients. *Clin. Chem.* **46,** 1703–1704 (2000).

40. De Paepe, B. & De Bleecker, J. L. Cytokines and Chemokines as Regulators of Skeletal Muscle Inflammation: Presenting the Case of Duchenne Muscular Dystrophy. *Mediators Inflamm.* **2013,** 1–10 (2013).
41. Messina, S. *et al.* Activation of NF-κB pathway in Duchenne muscular dystrophy: Relation to age. *Acta Myol.* **30,** 16–23 (2011).
42. Mendell, J. R. & Rodino-klapac, L. R. Duchenne muscular dystrophy : CRISPR / Cas9 treatment. *Nat. Publ. Gr.* **26,** 513–514 (2016).
43. Kodippili, K. *et al.* Nitric oxide-dependent attenuation of noradrenaline-induced vasoconstriction is impaired in the canine model of Duchenne muscular dystrophy. *J. Physiol. Soc.* **21,** 5199–5216 (2018).
44. Finsterer, J. & St, C. Heart Disease in Disorders of Muscle , Neuromuscular Transmission , and the Nerves. *Korean Circ. J.* **46,** 117–134 (2016).
45. Pantanowitz, L. Fat infiltration in the heart. *Heart* **85,** 253 (2001).
46. Hermans, M. C. E. *et al.* Neuromuscular Disorders Hereditary muscular dystrophies and the heart. *Neuromuscul. Disord.* **20,** 479–492 (2010).
47. Judge, Daniel P,Kass, David A, Thompson, Reid and Wagner, K. R. Pathophysiology_and_therapy_of cardiomyopathy in Duchenne muscular dystrophy. *Am. J. Cardiovasc. Drugs* **11,** 287–294 (2011).
48. Willmann, R., Possekel, S., Dubach-Powell, J., Meier, T. & Ruegg, M. A. Mammalian animal models for Duchenne muscular dystrophy. *Neuromuscul. Disord.* **19,** 241–249 (2009).
49. Yu, X., Bao, B., Echigoya, Y. & Yokota, T. Dystrophin-deficient large animal models: translational research and exon skipping. *Am. J. Transl. Res.* **7,** 1314–31 (2015).
50. Barthélémy, I. *et al.* Effects of an Immunosuppressive Treatment in the GRMD Dog Model of Duchenne Muscular Dystrophy. *PLoS One* **7,** 48478 (2012).
51. Winand, N. J., Edwards, M., Pradhan, D., Berian, C. A. & Cooper, B. J. Deletion of the dystrophin muscle promoter in feline muscular dystrophy. *Neuromuscul. Disord.* **4,** 433–445 (1994).
52. Al-Rewashdy, H., Ljubicic, V., Lin, W., Renaud, J. M. & Jasmin, B. J. Utrophin A is essential in mediating the functional adaptations of mdx mouse muscle following chronic AMPK activation. *Hum. Mol. Genet.* **24,** 1243–1255 (2015).
53. Deconinck, A. E. *et al.* Utrophin-dystrophin-deficient mice as a model for Duchenne muscular dystrophy. *Cell* **90,** 717–727 (1997).
54. Chen, H. C. *et al.* Utrophin Compensates dystrophin Loss during Mouse Spermatogenesis. *Sci. Rep.* **7,** 1–13 (2017).
55. Blanks, Glen B., Combs, Ariana C., Odom, Guy L., Bloch, Robert J., Chamberlain, J. S. Muscle structure influences utrophin expression in mdx mice. *PLoS One* **10,** 1004431 (2014).
56. Holland, A. *et al.* Proteomic profiling of cardiomyopathic tissue from the aged mdx model of Duchenne muscular dystrophy reveals a drastic decrease in laminin, nidogen and annexin. *Proteomics* **13,** 2312–2323 (2013).
57. Gutpell, K. M. *et al.* ANG1 treatment reduces muscle pathology and prevents a decline in perfusion in DMD mice. *PLoS One* **12,** 1–18 (2017).
58. Janssen, P. M. L., Hiranandani, N., Mays, T. A., Rafael-fortney, J. A. & Utrophin, J. A. R. Utrophin deficiency worsens cardiac contractile dysfunction present in

dystrophin-deficient mdx mice. *Am. J. Physiol. Circ. Physiol.* **289,** 2373–2378 (2005).

59. Bondoc, A. B. *et al.* Application of 3-D Echocardiography and Gated Micro-Computed Tomography to Assess Cardiomyopathy in a Mouse Model of Duchenne Muscular Dystrophy. *Ultrasound Med. Biol.* **40,** 2857–2867 (2014).
60. Kaspar, R. W., Candidate, R. N. F., Allen, H. D. & Montanaro, F. Current understanding and management of dilated cardiomyopathy in Duchenne and Becker muscular dystrophy. *J. Am. Acad. Nurse Pract.* **21,** 241–249 (2009).
61. Power, L. C. *et al.* Imaging the heart to detect cardiomyopathy in Duchenne muscular dystrophy : A review. *Neuromuscul. Disord.* **28,** 717–730 (2018).
62. Kirchmann, C., Kececioglu, D., Korinthenberg, R. & Dittrich, S. Echocardiographic and Electrocardiographic Findings of Cardiomyopathy in Duchenne and Becker – Kiener Muscular Dystrophies Cross-Sectional Investigation. *Pediatr. Cardiol.* **26,** 66–72 (2005).
63. Perloff, J. K. & Henze, Eberhard & Schelbert, H. Alterations in regional myocardial metabolism , perfusion , and wall motion in Duchenne muscular dystrophy studied by radionuclide imaging. *Circulation* **69,** 33–42 (1984).
64. Quinlivan, R. M. *et al.* Cardiac function, metabolism and perfusion in Duchenne and Becker muscular dystrophy. *Neuromuscul. Disord.* **6,** 237–246 (1996).
65. Hor, K. N., Mah, M. L., Johnston, P., Cripe, T. P. & Cripe, L. H. Advances in the diagnosis and management of cardiomyopathy in Duchenne muscular dystrophy. *Neuromuscul. Disord.* **28,** 711–716 (2018).
66. Shantsila, E. *et al.* IMproved exercise tolerance in patients with PReserved Ejection fraction by Spironolactone on myocardial fibrosiS in Atrial Fibrillation rationale and design of the IMPRESS-AF randomised controlled trial. *BMJ Open* **6,** e012241 (2016).
67. Van Putten, M. *et al.* Low dystrophin levels in heart can delay heart failure in mdx mice. *J. Mol. Cell. Cardiol.* **69,** 17–23 (2014).
68. Adachi, K. *et al.* Detection and management of cardiomyopathy in female dystrophinopathy carriers. *J. Neurol. Sci.* **386,** 74–80 (2018).
69. Hor, K. N., Mah, M. L., Johnston, P., Cripe, T. P. & Cripe, L. H. Advances in the diagnosis and management of cardiomyopathy in Duchenne muscular dystrophy. *Neuromuscul. Disord.* **28,** 711–716 (2018).
70. Finsterer, J., Stöllberger, C. & Towbin, J. A. Left ventricular noncompaction cardiomyopathy: Cardiac, neuromuscular, and genetic factors. *Nat. Rev. Cardiol.* **14,** 224–237 (2017).
71. Nelson, S. F. *et al.* Cardiac MRI biomarkers for Duchenne muscular dystrophy. *Biomark. Med.* **12,** 1271–1289 (2018).
72. Schuleri, Karl H., George, Richard T.& Lardo, A. C. Applications of cardiac multidetector CT beyond coronary angiography. *Nat. Rev. Cardiol.* **6,** 699–710 (2009).
73. Sayyed, S. H., Cassidy, M. M. & Hadi, M. A. Use of multidetector computed tomography for evaluation of global and regional left ventricular function. *J. Cardiovasc. Comput. Tomogr.* **3,** S23–S34 (2009).
74. de Graaf, F. R. *et al.* Clinical Application of CT Coronary Angiography: State of the Art. *Hear. Lung Circ.* **19,** 107–116 (2010).

75. Coats, C. J., Heywood, W. E., Mills, K. & Elliott, P. M. Current applications of biomarkers in cardiomyopathies. *Expert Rev. Cardiovasc. Ther.* **13,** 825–837 (2015).
76. Ameen, V. *et al.* Epidemiology of Idiopathic Dilated and Hypertrophic Cardiomyopathy. *J. Am. Coll. Cardiol.* **2,** 241–249 (2017).
77. Ameen, V. & Robson, L. G. Experimental Models of Duchenne Muscular Dystrophy : Relationship with Cardiovascular Disease. *Open Cardiovasc. Med. J.* **4,** 265–277 (2010).
78. Blondé-Cynober, F. *et al.* Diagnostic and prognostic value of brain natriuretic peptide (BNP) concentrations in very elderly heart disease patients: Specific geriatric cut-off and impacts of age, gender, renal dysfunction, and nutritional status. *Arch. Gerontol. Geriatr.* **52,** 106–110 (2011).
79. Tang, W. H. W. *et al.* Plasma B-Type Natriuretic Peptide Levels in Ambulatory Patients with Established Chronic Symptomatic Systolic Heart Failure. *Circulation* **108,** 2964–2966 (2003).
80. Mehra, M. R. *et al.* Obesity and suppressed B-type natriuretic peptide levels in heart failure. *J. Am. Coll. Cardiol.* **43,** 1590–1595 (2004).
81. Bhatt, A. S. *et al.* Interaction of body mass index on the association between N-terminal-pro-b-type natriuretic peptide and morbidity and mortality in patients with acute heart failure: Findings from ASCEND-HF (Acute Study of Clinical Effectiveness of Nesiritide in Decompens. *J. Am. Heart Assoc.* **7,** e006740 (2018).
82. Melanson, S. E. F., Tanasijevic, M. J. & Jarolim, P. Cardiac troponin assays: A view from the clinical chemistry laboratory. *Circulation* **116,** 501–504 (2007).
83. Schmid, J. *et al.* Elevated Cardiac Troponin T in Patients With Skeletal Myopathies. *J. Am. Coll. Cardiol.* **71,** 1540–1549 (2018).
84. Rittoo, D., Jones, A., Lecky, B. & Neithercut, D. Elevation of cardiac troponin T, but not cardiac troponin I, in patients with neuromuscular diseases: Implications for the diagnosis of myocardial infarction. *J. Am. Coll. Cardiol.* **63,** 2411–2420 (2014).
85. Kojima, M. & Kangawa, K. Ghrelin: Structure and Function. *Physiol. Rev.* **85,** 495–522 (2005).
86. Müller, T. D. *et al.* Ghrelin. *Mol. Metab.* **4,** 437–460 (2015).
87. Großauer, J., Kosol, S., Schrank, E. & Zangger, K. The peptide hormone ghrelin binds to membrane-mimetics via its octanoyl chain and an adjacent phenylalanine. *Bioorganic Med. Chem.* **18,** 5483–5488 (2010).
88. Delporte, C. Structure and Physiological Actions of Ghrelin. *Scientifica (Cairo).* **2013,** 1–25 (2013).
89. Lilleness, B. M. & Frishman, W. H. Ghrelin and the Cardiovascular System. *Cardiol. Rev.* **24,** 288–297 (2016).
90. Katugampola, S. D., Pallikaros, Z. & Davenport, A. P. [125 I- His 9] -Ghrelin , a novel radioligand for localizing GHS orphan receptors in human and rat tissue ; up-regulation of receptors with atherosclerosis. *Br. J. Pharmacol.* **134,** 143–149 (2001).
91. Tesauro, M., Schinzari, F., Caramanti, M., Lauro, R. & Cardillo, C. Metabolic and Cardiovascular Effects of Ghrelin. *Int. J. Pept.* **2010,** 1–7 (2010).
92. Shimizu, Y. *et al.* Ghrelin improves endothelial dysfunction through growth

hormone-independent mechanisms in rats. *Biochem. Biophys. Res. Commun.* **310,** 830–835 (2003).
93. Iglesias, M. J. *et al.* Growth hormone releasing peptide (ghrelin) is synthesized and secreted by cardiomyocytes. *Cardiovasc. Res.* **62,** 481–488 (2004).
94. Yuan, M. *et al.* GHSR-1a is a novel pro-angiogenic and anti-remodeling target in rats after myocardial infarction. *Eur. J. Pharmacol.* **788,** 218–225 (2016).
95. Yuan, M. J. I. E., Huang, H. E. & Huang, C. X. I. N. Potential new role of the GHSR - 1a - mediated signaling pathway in cardiac remodeling after myocardial infarction (Review). *Oncol. Lett.* **8,** 969–971 (2014).
96. Wang, L., Chen, Q., Li, G. & Ke, D. Ghrelin stimulates angiogenesis via GHSR1a-dependent MEK/ERK and PI3K/Akt signal pathways in rat cardiac microvascular endothelial cells. *Peptides* **33,** 92–100 (2012).
97. Baldanzi, G. *et al.* Ghrelin and des-acyl ghrelin inhibit cell death in cardiomyocytes and endothelial cells through ERK1/2 and PI 3-kinase/AKT. *J. Cell Biol.* **159,** 1029–1037 (2002).
98. Frascarelli, S., Ghelardoni, S., Ronca-Testoni, S. & Zucchi, R. Effect of ghrelin and synthetic growth hormone secretagogues in normal and ischemic rat heart. *Basic Res. Cardiol.* **98,** 401–405 (2003).
99. Soeki, T. *et al.* Ghrelin suppresses cardiac sympathetic activity and prevents early left ventricular remodeling in rats with myocardial infarction. *Am. J. Physiol. Circ. Physiol.* **294,** H426–H432 (2007).
100. Lacerda-Miranda, G. *et al.* Ghrelin signaling in heart remodeling of adult obese mice. *Peptides* **35,** 65–73 (2012).
101. Nagaya, N. *et al.* Chronic administration of ghrelin improves left ventricular dysfunction and attenuates development of cardiac cachexia in rats with heart failure. *Circulation* **104,** 1430–1435 (2001).
102. Nagaya, N. *et al.* Hemodynamic and hormonal effects of human ghrelin in healthy volunteers. *Am. J. Physiol. Regul. Integr. Comp. Physiol.* **280,** R1483-7 (2001).
103. Nagaya, N. *et al.* Effects of ghrelin administration on left ventricular function, exercise capacity, and muscle wasting in patients with chronic heart failure. *Circulation* **110,** 3674–3679 (2004).
104. Iantorno, M. *et al.* Ghrelin has novel vascular actions that mimic PI 3-kinase-dependent actions of insulin to stimulate production of NO from endothelial cells. *Am. J. Physiol. Endocrinol. Metab.* **292,** 756–64 (2007).
105. Tesauro, M. *et al.* Ghrelin improves endothelial function in patients with metabolic syndrome. *Circulation* **112,** 2986–2992 (2005).
106. Xiang, Y. *et al.* Ghrelin inhibits AGEs-induced apoptosis in human endothelial cells involving ERK1/2 and PI3K/Akt pathways. *Cell Biochem. Funct.* **29,** 149–155 (2011).
107. Chow, K. B. S., Cheng, C. H. K. & Wise, H. Anti-inflammatory activity of ghrelin in human carotid artery cells. *Inflammation* **32,** 402–409 (2009).
108. Li, W. G. *et al.* Ghrelin Inhibits Proinflammatory Responses and Nuclear Factor-κB Activation in Human Endothelial Cells. *Circulation* **109,** 2221–2226 (2004).
109. Dixit, V. D. *et al.* Ghrelin inhibits leptin- and activation-induced proinflammatory cytokine expression by human monocytes and T cells. *J. Clin. Invest.* **114,** 57–66 (2004).

110. Granado, M., Priego, T., Martín, A. I., Villanúa, M. Á. & López-Calderón, A. Anti-inflammatory effect of the ghrelin agonist growth hormone-releasing peptide-2 (GHRP-2) in arthritic rats. *Am. J. Physiol. Metab.* **288,** E486–E492 (2004).
111. Huang, C. X. *et al.* Ghrelin inhibits post-infarct myocardial remodeling and improves cardiac function through anti-inflammation effect. *Peptides* **30,** 2286–2291 (2009).
112. Douglas, G. A. F. *et al.* Characterization of a far-red analog of ghrelin for imaging GHS-R in P19-derived cardiomyocytes. *Peptides* **54,** 81–88 (2014).
113. Sullivan, R. *et al.* Changes in the Cardiac GHSR1a-Ghrelin System Correlate With Myocardial Dysfunction in Diabetic Cardiomyopathy in Mice. *J. Endocr. Soc.* **2,** 178–189 (2018).
114. Sullivan, R. *et al.* Dynamics of the Ghrelin/Growth Hormone Secretagogue Receptor System in the Human Heart Before and After Cardiac Transplantation. *J. Endocr. Soc.* **3,** 748–762 (2019).
115. McDonald, A. A., Hebert, S. L., Kunz, M. D., Ralles, S. J. & McLoon, L. K. Disease course in mdx:Utrophin+/−mice: comparison of three mouse models of duchenne muscular dystrophy. *Physiol. Rep.* **3,** 1–22 (2015).
116. Shi, S. R., Liu, C. & Taylor, C. R. Standardization of immunohistochemistry for formalin-fixed, paraffin-embedded tissue sections based on the antigen-retrieval technique: From experiments to hypothesis. *J. Histochem. Cytochem.* **55,** 105–109 (2007).
117. Papademetriou, Jason, Garnacho Carmen, Serrano Daniel , Bhowmick Tridib, Edward H. Schuchman, and M. S. lysosomal enzymes to ICAM-1 versus transferrin receptor. *J. Inherit Metab. Disord.* **36,** 467–477 (2014).
118. Angin, Y., Schwenk, R. W., Glatz, J. F. C., Luiken, J. J. F. P. & Steinbusch, L. K. M. CD36 as a target to prevent cardiac lipotoxicity and insulin resistance. *Prostaglandins, Leukot. Essent. Fat. Acids* **88,** 71–77 (2012).
119. Lawson, C. & Wolf, S. ICAM-1 signaling in endothelial cells. *Pharmacol. Reports* **61,** 22–32 (2009).
120. Frank, P. G. & Lisanti, M. P. ICAM-1: role in inflammation and in the regulation of vascular permeability. *Am. J. Physiol. Circ. Physiol.* **295,** H926–H927 (2008).
121. Gutpel, K. M., Hrinivich, W. T. & Hoffman, L. M. Skeletal muscle fibrosis in the mdx/utrn+/-mouse validates its suitability as a murine model of duchenne muscular dystrophy. *PLoS One* **10,** 1–13 (2015).
122. Kinali, M. *et al.* Muscle histology vs MRI in Duchenne muscular dystrophy. *Neurology* **76,** 346–353 (2011).
123. Diniz, G. The Histopathological Features of Muscular Dystrophies. *Muscular Dystrophy* **4,** 1–18 (2016).
124. Bell, C. D. & Conen, P. E. Histopathological changes in Duchenne muscular dystrophy . *Journal of the Neurological Sciences* **7,** 529–544 (1968).
125. Mcnally, E. Cardiomyopathy in Muscular Dystrophy : When to treat ? *JAMA Cardiol.* **2,** 199 (2017).
126. Wahbi, K. Aspects cardiologiques des dystrophinopathies. *Arch. Pédiatrie* **22,** 12S37-12S41 (2016).
127. Jokinen, M. P., Lieuallen, W. G., Johnson, C. L., Dunnick, J. & Nyska, A. Characterization of spontaneous and chemically induced cardiac lesions in rodent

model systems: The National Toxicology Program experience. *Cardiovasc. Toxicol.* **5,** 227–244 (2005).
128. Legge, C. H. *et al.* Histological Characterization of Dilated Cardiomyopathy in the Juvenile Toy Manchester Terrier. *Vet. Pathol.* **50,** 1043–1052 (2013).
129. Clausell, N. *et al.* Myocardial vacuolization, a marker of ischemic injury, in surveillance cardiac biopsies posttrans plant: Correlations with morphologic vascular disease and endothelial dysfunction. *Cardiovasc. Pathol.* **5,** 29–37 (1996).
130. Kellman, P., Hernando, D. & Arai, A. E. Myocardial Fat Imaging. *Curr. Cardiovasc. Imaging Rep.* **3,** 83–91 (2010).
131. Mavrogeni, S. *et al.* Myocardial inflammation in Duchenne Muscular Dystrophy as a precipitating factor for heart failure : a prospective study. *BMC Neurol.* **10,** 1–7 (2010).
132. asinger, R. W., Mikell, F. L., Sharma, B. & Hodges, M. Observations on detecting left ventricular thrombus with two dimensional echocardiography: emphasis on avoidance of false positive diagnoses. *Am. J. Cardiol.* **47,** 145–156 (1981).
133. Yokota Y, Kawanishi H, Hayakawa M, Kumaki T, Takarada A, Nakanishi O, F. H. Cardiac thrombus in dilated cardiomyopathy. Relationship between left ventricular pathophysiology and left ventricular thrombus. *Jpn Hear. J.* **30,** 1–11 (1989).
134. Mohammed Baba Abdulkadir, Olayinka Rasheed Ibrahim, Folake Moriliat Afolayan, and O. T. A. Left Ventricular Outflow Tract Thrombus in a Child with Dilated Cardiomyopathy: An Atypical Location. *J Cardiovasc Echogr* **27,** 101–103 (2017).
135. Nitahara-Kasahara, Y., Takeda, S. & Okada, T. Inflammatory predisposition predicts disease phenotypes in muscular dystrophy. *Inflamm. Regen.* **36,** 3–7 (2017).
136. Zhu, Y. *et al.* Identification of different macrophage subpopulations with distinct activities in a mouse model of oxygen-induced retinopathy. *Int. J. Mol. Med.* **40,** 281–292 (2017).
137. Giordano, C. *et al.* Toll-like receptor 4 ablation in mdx mice reveals innate immunity as a therapeutic target in Duchenne muscular dystrophy. *Hum. Mol. Genet.* **24,** 2147–2162 (2015).
138. Riad, A. *et al.* Variants of toll-like receptor 4 predict cardiac recovery in patients with dilated cardiomyopathy. *J. Biol. Chem.* **287,** 27236–27243 (2012).
139. Lee, J. H., Buras, E. D., Yu, K., Wang, R. & Smith, C. W. Ghrelin receptor regulates adipose tissue inflammation in aging. *Aging (Albany. NY).* **8,** 178–191 (2016).
140. Li, B. *et al.* Ghrelin protects alveolar macrophages against lipopolysaccharide-induced apoptosis through growth hormone secretagogue receptor 1a-dependent c-jun n-terminal kinase and wnt/ß-catenin signaling and suppresses lung inflammation. *Endocrinology* **156,** 203–217 (2015).
141. Cruz-guzmán, O. R., Rodríguez-cruz, M., Elena, R. & Cedillo, E. Systemic Inflammation in Duchenne Muscular Dystrophy : Association with Muscle Function and Nutritional Status. *BioMed Reserach Int.* **2015,** 1–7 (2015).
142. Stenvinkel, P. *et al.* IL-10, IL-6, and TNF-α: Central factors in the altered cytokine network of uremia - The good, the bad, and the ugly. *Kidney Int.* **67,** 1216–1233

(2005).
143. Fontes, J. A., Rose, N. R. & Daniela, C. Cytokine The varying faces of IL-6 : From cardiac protection to cardiac failure. *Cytokine* **74,** 62–68 (2015).
144. Palladino, M. *et al.* Angiogenic Impairment of the Vascular Endothelium. *Arterioscler. Thromb. Vasc. Biol.* **33,** 2867–2876 (2013).
145. Febbraio, M. & Silverstein, R. L. CD36: Implications in cardiovascular disease. *Int. J. Biochem. Cell Biol.* **39,** 2012–2030 (2007).
146. Koonen, D. P. Y. *et al.* CD36 expression contributes to age-induced cardiomyopathy in mice. *Circulation* **116,** 2139–2147 (2007).
147. Honkura, N. *et al.* Intravital imaging-based analysis tools for vessel identification and assessment of concurrent dynamic vascular events. *Nat. Commun.* **9,** 1–10 (2018).
148. Wu, Z. *et al.* Multi-photon microscopy in cardiovascular research. *Methods* **130,** 79–89 (2017).
149. Reano, S., Graziani, A. & Filigheddu, N. Acylated and unacylated ghrelin administration to blunt muscle wasting. *Curr. Opin. Clin. Nutr. Metab. Care* **17,** 236–40 (2014).
150. Porporato, P. E. *et al.* Acylated and unacylated ghrelin impair skeletal muscle atrophy in mice. *J. Clin. Invest.* **123,** 611–622 (2013).
151. Togliatto, G. *et al.* Unacylated ghrelin promotes skeletal muscle regeneration following hindlimb ischemia via SOD-2-mediated miR-221/222 expression. *J. Am. Heart Assoc.* **2,** 1–21 (2013).

Appendix A. Animal research ethics approval

Western

AUP Number: [redacted]
PI Name: Hoffman, Lisa M
AUP Title: Hoffman Breeding Protocol
Approval Date: [redacted]

Official Notice of Animal Use Subcommittee (AUS) Approval: Your new Animal Use Protocol (AUP) entitled "Hoffman Breeding Protocol" has been APPROVED by the Animal Use Subcommittee of the University Council on Animal Care. This approval, although valid for four years, and is subject to annual Protocol Renewal. [redacted]

1. This AUP number must be indicated when ordering animals for this project.
2. Animals for other projects may not be ordered under this AUP number.
3. Purchases of animals other than through this system must be cleared through the ACVS office. Health certificates will be required.

The holder of this Animal Use Protocol is responsible to ensure that all associated safety components (biosafety, radiation safety, general laboratory safety) comply with institutional safety standards and have received all necessary approvals. Please consult directly with your institutional safety officers.

Submitted by: Copeman, Laura
on behalf of the Animal Use Subcommittee
University Council on Animal Care

MAEDEH NAGHIBOSADAT CV

Education

2017-2019 Master of Pathology

University of Western Ontario

2013-2014 Master of Biotechnology

University of Queensland

2005 – 2009 Bachelor's Degree in microbiology

Tehran Medical university

Work Experience

Jan 2017-Now: Lawson Health Research Institute **London, Ontario**

Jan 2013-Jan2016: Institute for Molecular Biosciences (IMB) **Brisbane, Australia**

Research Assistant in Professor Alpha Yap Lab (Jan 2013- Jan2016)

July 2013-June 2014: Australian Institute for Bioengineering and Nanotechnology (AIBN)

Master's Project in Professor Matt Trau Lab **Brisbane, Australia**

2011 – 2012: Velenjak Clinical Laboratory **Tehran, Iran**

Laboratory Assistant

2011 – 2012: Taleghani Hospital **Tehran, Iran**

Laboratory Assistant

2010 – 2011: Biotechnology Research Centre, Islamic Azad University **Tehran, Iran**

Laboratory Assistant

2009: Pasteur Institute of Iran (Production and Research Complex) **Tehran, Iran**

Professional Internship

2006– 2007: Biochemistry laboratory at Tehran University **Tehran, Iran**

Professor's Assistant

Additional Training and awards

- Molecular Imaging Travel award -University of Western Ontario. July 2108
- Teaching assistant at University of Western Ontario. September 2017-April 2018 Interdisciplinary Medical Sciences (4900F/G Lab course)
- Motivational Interviewing and Coaching Training Certificate 2018
- Capacity Planning in Canadian Health Care Training Certificate 2018
- Financial accounting in Canadian Health Care Training Certificate 2018
- Transdisciplinary Bone and Joint award/University of Western Ontario 2017
- Dean's Commendation for high achievement in 2014 Faculty of Science UQ
- Teaching assistant at University of Queensland. February 2014- June 2014 Molecular Biology Lab course
- Research scholar award in winter 2014 Faculty of Science UQ
- Research scholar award in summer 2013 Faculty of Science UQ
- Lecturing Certificate in Tissue Engineering workshop in 2011 Pasteur Institute

---

Presentations:

- *Characterization of Growth Hormone Secretagogue Receptor (GHSR) in a model of dilated cardiomyopathy*. Canadian Connective Tissue Congress 2019/Canada.
- *Ghrelin receptor alteration in cardiovascular inflammation in Duchenne muscular dystrophy*. Children's Research Day 2019/Canada.
- *Characterization of Growth Hormone Secretagogue Receptor (GHSR) in a model of Dilated Cardiomyopathy*. Pathology Research Day 2019/Canada
- *Anillin promotes cell contractility by cyclic resetting of RhoA*. Hunter Cell Biology Meeting 2019/Australia
- *Ghrelin & des-acyl ghrelin binding in cardiac tissue are altered with cardiovascular inflammation in Duchenne muscular dystrophy*. Canadian Cardiovascular Congress 2018/Canada.
- *Ghrelin & des-acyl ghrelin binding in cardiac tissue are altered with cardiovascular inflammation in Duchenne muscular dystrophy*. Canadian Cardiovascular Congress 2018/Canada.
- *Alterations in ghrelin and GHSR with cardiovascular inflammation in Duchenne muscular dystrophy*. World Microcirculation Congress 2018/Canada.
- *Characterization of GHSR as a biomarker of cardiac inflammation*. Bone & Joint Conference 2018/Canada
- *Characterization of GHSR as a biomarker of cardiac inflammation*. Cellular & Molecular Imaging Symposium 2018/Canada
- *Characterization and the role of Ghrelin & its' receptor in the vasculature of Duchenne Muscular Dystrophy*. London Health Research Day 2018/Canada
- *Characterization and the role of Ghrelin & its' receptor in the vasculature of Duchenne Muscular Dystrophy*. Pathology Research Day 2018/Canada
- *Anillin Promotes Cell Contractility in adherens Junction via RhoA*. An international forum for cell biology/EMBO 2017/US
- *The relation between Anillin, RhoA & E-cadherin*. International Congress of Cell Biology 2018/India

- *Dynamic cortical binding promotes RhoA flux to effectors for cellular contractility*.IMB Symposium 2016/Australia
- *Anillin stabilizes active RhoA at adherens junctions for productive signaling*. International Gordon Research Conference 2016/US
- *Anillin stabilizes active RhoA at adherens junctions for productive signaling*. International Cell Biology Conference 2015/India
- *Detecting Exosomes Specifically: A Multiplex Device based on Alternating Current Electrohydrodynamics Induced Nanoshearing*. International MicroTAS Conference 2014/Germany
- *Detecting Exosome specifically*. International Nanobio Conference 2014/Australia

---

Publications:

1. **Naghibosadat, M**.; Vaidyanathan, R.; Rauf, S.; Korbie, D.; Carrascosa,L.G.; Shiddiky, M. J. A.; Trau, M. **2014**, Analytical Chemistry Journal. *Detecting Exosomes Specifically: A Multiplex Device based on Alternating Current Electrohydrodynamics Induced Nanoshearing*

2. Budnar, S.; Kabir,H.;Gomez,G.;**Naghibosadat, M**.; Verma, S.;Hamilton,N.;Morris,R.and Yap, A. S. **2019**, Developmental Cell.*Anillin Promotes Cell Contractility by Cyclic Resetting of RhoA*

3. Budnar, S.; Kabir,H.;Gomez,G.;**Naghibosadat, M**.; Verma, S.; Hamilton,N and Yap, A. S. **2018**, Biorxiv. *Scaffolding of RhoA contractile signaling by anillin: a regulatory analogue of kinetic proofreading* . **doi:** https://doi.org/10.1101/282756

4. Budnar, S.; **Naghibosadat, M**.; Visanoff, V.; and Yap, A. S., *Light induced approach to control the signaling at cell-cell junction* (Under revision)

5. **Naghibosadat, M**.; Luyt, L.; Hoffman L.; Dhanvantari S.; *Alterations in ghrelin and GHSR with cardiovascular inflammation in Duchenne muscular dystrophy* (Manuscript in preparation)

---

6. Priya, R.; Gomez, G. A.; Budnar, S.; Verma, S.; Cox, H. L.; Hamilton, N.; and Yap, A. S.;**2015**, Nature Cell Biology. *Feedback regulation through myosin II confers robustness on RhoA signalling at E-cadherin junctions.* (**Acknowledged** for cloning and generating reagents)
7. Hou, J.; Kovacs, M.; Dhanvantari, S.; Luyt, L. ;**2018,** J.Med.Chem. *Development of Candidates for Positron Emission Tomography (PET) Imaging of Ghrelin Receptor in Disease: Design, Synthesis, and Evaluation of Fluorine-Bearing Quinazolinone Derivatives.* (**Acknowledged** for cell and transfection work)